HHS Public Access

Author manuscript

J Physiol. Author manuscript; available in PMC 2022 April 11.

Published in final edited form as:

J Physiol. 2021 December ; 599(23): 5179–5201. doi:10.1113/JP281707.

The V2475F CPVT1 mutation yields distinct RyR2 channel populations that differ in their responses to cytosolic Ca^{2+} and Mg^{2+}

Abigail D. Wilson[1], **Jianshu Hu**[1], **Charalampos Sigalas**[1,*], **Elisa Venturi**[1], **Héctor H. Valdivia**[2], **Carmen R. Valdivia**[2], **Ming Lei**[1], **Maria Musgaard**[3], **Rebecca Sitsapesan**[1,*]

[1]Department of Pharmacology, University of Oxford, UK;

[2]Department of Medicine, Division of Cardiovascular Medicine, University of Wisconsin School of Medicine and Public Health, Madison, USA;

[3]Department of Chemistry and Biomolecular Sciences, University of Ottawa, Canada.

Abstract

Catecholaminergic polymorphic ventricular tachycardia type 1 (CPVT1) is a lethal genetic disease causing arrhythmias and sudden cardiac death in children and young adults and is linked to mutations in the cardiac ryanodine receptor (RyR2). The effects of CPVT1 mutations on RyR2 ion-channel function are often investigated using purified recombinant RyR2 channels homozygous for the mutation. However, CPVT1 patients are heterozygous for the disease, so this approach does not reveal the true changes to RyR2 function across the entire RyR2 population of channels in the heart. We therefore investigated the native cardiac RyR2 single-channel abnormalities in mice heterozygous for the CPVT1 mutation, V2475F(+/−)-RyR2, and

* *Co-corresponding authors* .

Author Contribution: Abigail Wilson: Conception or design of the work; Acquisition or analysis or interpretation of data for the work; Drafting the work or revising it critically for important intellectual content; Final approval of the version to be published; Agreement to be accountable for all aspects of the work Jianshu Hu: Conception or design of the work; Acquisition or analysis or interpretation of data for the work; Drafting the work or revising it critically for important intellectual content; Final approval of the version to be published; Agreement to be accountable for all aspects of the work Charalampos Sigalas: Conception or design of the work; Acquisition or analysis or interpretation of data for the work; Drafting the work or revising it critically for important intellectual content; Final approval of the version to be published; Agreement to be accountable for all aspects of the work Elisa Venturi: Conception or design of the work; Acquisition or analysis or interpretation of data for the work; Drafting the work or revising it critically for important intellectual content; Final approval of the version to be published; Agreement to be accountable for all aspects of the work Héctor Valdivia: Conception or design of the work; Acquisition or analysis or interpretation of data for the work; Drafting the work or revising it critically for important intellectual content; Final approval of the version to be published; Agreement to be accountable for all aspects of the work Carmen Valdivia: Conception or design of the work; Acquisition or analysis or interpretation of data for the work; Drafting the work or revising it critically for important intellectual content; Final approval of the version to be published; Agreement to be accountable for all aspects of the work Ming Lei: Conception or design of the work; Acquisition or analysis or interpretation of data for the work; Drafting the work or revising it critically for important intellectual content; Final approval of the version to be published; Agreement to be accountable for all aspects of the work Maria Musgaard: Conception or design of the work; Acquisition or analysis or interpretation of data for the work; Drafting the work or revising it critically for important intellectual content; Final approval of the version to be published; Agreement to be accountable for all aspects of the work Rebecca Sitsapesan: Conception or design of the work; Acquisition or analysis or interpretation of data for the work; Drafting the work or revising it critically for important intellectual content; Final approval of the version to be published; Agreement to be accountable for all aspects of the work

Author Contributions

ADW, JH and EV performed the experiments. ADW, JH, CS and EV analysed the data. HHV and CRV generated and provided the animal model. RS supervised the project and wrote the manuscript. All authors contributed to the final version of the paper.

Competing Interests

None of the authors have any conflicts of interest.

applied molecular modelling techniques to investigate the possible structural changes that could initiate any altered function. We observed that increased sensitivity of cardiac V2475F(+/−)-RyR2 channels to both activating and inactivating levels of cytosolic Ca^{2+}, plus attenuation of Mg^{2+} inhibition, were the most marked changes. Severity of abnormality was not uniform across all channels, giving rise to multiple sub-populations with differing functional characteristics. For example, 46% of V2475F(+/−)-RyR2 channels exhibited reduced Mg^{2+} inhibition and 23% were actually activated by Mg^{2+}. Using homology modelling, we discovered that V2475 is situated at a hinge between two regions of the RyR2 helical-domain-1 (HD1). Our model proposes that detrimental functional changes to RyR2 arise because mutation at this critical site reduces the angle between these regions. Our results demonstrate the necessity of characterising the total heterozygous population of CPVT1-mutated channels in order to understand CPVT1 phenotypes in patients.

Graphical Abstract

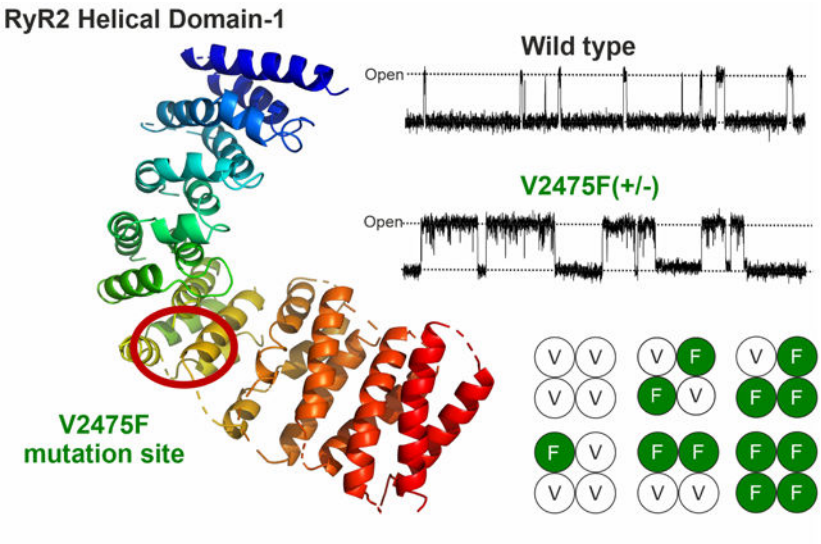

(Left) RyR2 Helical Domain-1 with the V2475F mutation site indicated by the red circle. (Top right) Typical RyR2 single-channel recordings highlighting the increased opening burst durations of RyR2 isolated from V2475F(+/−) hearts compared to wild type hearts. (Bottom right) Possible RyR2 tetramer formations in V2475F(+/−) hearts. White (V) and green (F) circles represent wild type and mutated monomers, respectively.

Keywords

RyR2; single-channel; catecholaminergic polymorphic ventricular tachycardia; sarcoplasmic reticulum Ca^{2+} release

Introduction

The cardiac isoform of the sarcoplasmic reticulum (SR) ryanodine receptor (RyR2) is the primary Ca^{2+}-release channel in the heart (Rousseau *et al.*, 1986). The unique gating

and ion conducting properties of RyR2 are essential for maintaining appropriate SR Ca^{2+} release during cardiac excitation-contraction (EC) coupling so that the heart can beat in a rhythmic fashion. The signal that triggers the coordinated opening of RyR2 channels across all the individual muscle cells of the heart is a rise in cytosolic [Ca^{2+}] (Fabiato, 1983; Näbauer *et al.*, 1989; Bers, 2002). However, the resultant increase in open probability (Po) of RyR2 is dependent on many other physiological factors, not least on the many ligands that, in synergy with cytosolic Ca^{2+}, regulate RyR2 gating (Meissner & Henderson, 1987; Sitsapesan & Williams, 1994a; Kermode *et al.*, 1998). Anything that perturbs this complex regulatory system has the potential to disrupt cardiac SR Ca^{2+} release with lethal consequences. This is exemplified in catecholaminergic polymorphic ventricular tachycardia (CPVT), a disease caused by mutations to RyR2 or associated proteins which can be acquired in an autosomal dominant or recessive manner (Lahat *et al.*, 2001; Priori *et al.*, 2001; Laitinen *et al.*, 2001). When the disease is linked to mutations in RyR2, it is termed CPVT type 1 (CPVT1) and is autosomal dominant (Priori *et al.*, 2001). Typically, patients have a normal baseline ECG, sometimes exhibiting bradycardia, but without any evidence of cardiac structural abnormality (Priori *et al.*, 2002). Upon physical exertion or during emotional stress, premature ventricular beats can arise leading to polymorphic ventricular tachycardia and ventricular fibrillation (Napolitano *et al.*, 2016). Early diagnosis is important because mortality among children and young adults is high when untreated (Swan *et al.*, 1999; Priori *et al.*, 2002).

There is growing awareness that symptoms additional to adrenergic stress-induced ventricular arrhythmias are linked to mutations in RyR2. These include supra-ventricular arrhythmias (Else *et al.*, 2012) and structural changes to the heart that are associated with specific types of cardiomyopathy (Bhuiyan *et al.*, 2007; Denegri *et al.*, 2014; Lavorato *et al.*, 2017; Roston *et al.*, 2017; Bongianino *et al.*, 2017; Alvarado *et al.*, 2019; Nozaki *et al.*, 2020). That such a range of symptoms arise from mutations to RyR2 suggests that different mutations produce distinct functional changes to the gating and/or conductance of RyR2. In turn, this leads to different abnormalies of SR Ca^{2+} release and the development of divergent cardiac problems and there are an increasing number of reports detailing the clinical phenotypes, for example Priori & Chen (2011) (Priori & Chen, 2011). Altered patterns of SR Ca^{2+} release and the characteristics of catecholamine-induced arrhythmias in mouse models of CPVT are also frequently studied. However, there is a paucity of information describing the detailed alterations to RyR2 single-channel function that occur in the various RyR2 mutations that cause life-threatening disease. CPVT1 is generally thought to be caused by ‘leaky’ RyR2 channels that have an increased sensitivity to cytosolic or luminal Ca^{2+} (Jiang *et al.*, 2005; Liu *et al.*, 2006; Xiao *et al.*, 2016; Uehara *et al.*, 2017) or which are ‘hyperphosphorylated’ (Marx *et al.*, 2000; Wehrens *et al.*, 2003; Lehnart *et al.*, 2004) but these generalised descriptions are too vague to enable the design of effective treatments that are suitable to treat the divergent symptoms of the patients.

The problem is partly due to the difficulties of isolating sufficient RyR2 protein from the tiny hearts of CPVT mouse models to incorporate into planar phospholipid bilayers for single-channel studies. Most of our understanding of CPVT-induced changes to RyR2 function has been obtained using membrane preparations enriched with RyR2 from mouse hearts using detergent or, more commonly, using recombinantly expressed RyR2 (Liu *et*

al., 2013; Uehara *et al.*, 2017). It is known that use of detergent can affect the gating of RyR channels (Beard *et al.*, 2002; Györke *et al.*, 2004) and so this should be avoided for functional studies. Using recombinant RyR2 has additional problems. Importantly, the mutation will be present in all of the four monomers that make up the RyR2 tetrameric ion channel. However, CPVT1 is an autosomal dominant condition. Patients are heterozygous for the mutation and so only a small fraction of the total population of channels present in the heart will have four mutated monomers. Fig. 1 illustrates the expected likelihood of various RyR2 subunit compositions for a patient with CPVT1.

To begin addressing the above problems, we have isolated SR vesicles from the hearts of mice, heterozygous for the V2475F mutation which is associated with CPVT1 in humans, and incorporated these into bilayers to record single RyR2 channel currents. We have investigated if the effects of the four most important RyR2 regulatory ligands (cytosolic Ca^{2+}, luminal Ca^{2+}, cytosolic Mg^{2+} and ATP) are altered. We have also examined whether monovalent and divalent cation conductance and the relative Ca^{2+}: K^{+} permeability is affected. We have recorded an unprecedented number of single-channel experiments which has allowed us to investigate changes in function among the different sub-populations of the V2475F(+/−) RyR2 channels in the heart. V2475 resides in the RyR2 helical domain 1 (HD1) and neighbours R2474, a residue also known to be a CPVT1 mutation site (Jiang *et al.*, 2005; Lehnart *et al.*, 2008). Peng et al. (2016) show that this is a flexible region with the potential to influence neighbouring domains and regulate distant parts of the RyR2 protein (Peng *et al.*, 2016). Using molecular modelling we have therefore compared the possible structural changes induced by the V2475F and R2474S mutations. Our study shows that the V2475F-RyR2 mutation causes very specific alterations to single-channel conductance and ligand regulation. Furthermore, by characterising the overall population of channels derived from the hearts of V2475F(+/−) mice we have identified sub-populations of RyR2 that display graded changes in their response to cytosolic Ca^{2+} and Mg^{2+}.

Methods

Ethical Approval

All procedures have been approved by the University of Oxford Ethical Review Committee (Pharmacology and Biochemistry subcommittee, approval ref. PPL: 30–3340) in strict accordance with the relevant United Kingdom Animals (Scientific Procedures) Act 1986 Home Office and institutional guidelines and regulations. The authors confirm that they have taken all steps to minimise the animals' pain and suffering. This work complies with the Journal's animal ethics checklist (Grundy, 2015).

Animal Information

Heterozygote RyR2-V2475F Knock-In (RyR2-V2475F(+/−)) C57BL/6J mice and wild-type (WT) littermates were kindly provided by Hector Valdivia from the University of Wisconsin (Loaiza *et al.*, 2013), and were housed in individually ventilated cages in a pathogen-free facility at the University of Oxford. Mice were maintained in a 12 h light/dark cycle and given *ad libitum* access to normal chow and water. The use of mice was shared between members of the laboratory, in which cardiac and other tissues were taken from the same

mouse wherever possible to comply with the “three Rs” principles (Fenwick *et al.*, 2009). Isolated mixed membrane vesicles were prepared from 5 female and 5 male hearts from RyR2-V2475F(+/−) or WT littermates between 10–13 weeks old. Mice were humanely killed by cervical dislocation in line with ASPA Schedule 1 and the Journal’s ethical standards. The use of sedatives or anaesthetic agents were avoided to minimise confounding effects on the tissues obtained from the mice. For each intervention, data were collected using at least 3 membrane preparations (therefore 30 animals total).

Isolation of mixed membrane from mouse cardiac tissue

Isolated mixed membrane vesicles were prepared using methods described previously (El-Ajouz *et al.*, 2017). Briefly, mouse cardiac tissue was dissected and snap frozen. Frozen tissue was finely homogenised in a buffer containing 300 mM sucrose, 20 mM K^+ piperazine-N,N′-bis(2-ethanesulfonic acid) (KPIPES), 5 mM sodium fluoride (NaF), 2.5 mM dithiothreitol (DTT), 1 mM phenylmethylsulfonyl fluoride (PMSF), supplemented with a protease inhibitor cocktail, pH 7.2. The tissue homogenate was centrifuged at 6,000 g for 20 min at 4°C. The supernatant obtained was centrifuged at 120,000 g for 1 h at 4°C to pellet the membrane fraction. This was resuspended in 400 mM sucrose, 5 mM Tris/HEPES, 5 mM NaF at pH 7.2. The preparation was snap frozen and stored at −80°C.

Single-channel recordings

RyR2 channels were incorporated into planar phospholipid bilayers as previously described (Sitsapesan *et al.*, 1991) in a 1:1 mixture of phosphatidylethanolamine: phosphatidylserine (PE:PS) (Avanti Lipids). With Ca^{2+} as the permeant ion, current fluctuations through RyR2 channels were recorded under voltage-clamp conditions in solutions of 250 mM HEPES, 80 mM Tris, pH 7.2, buffered with 1 mM EGTA to 100 nM – 10 mM Ca^{2+} on the cytosolic side, and 250 mM glutamic acid, 10 mM HEPES, pH to 7.2 with $Ca(OH)_2$ (free Ca^{2+} approximately 50 mM) on the luminal side. The luminal chamber was voltage-clamped at ground and the cytosolic chamber was clamped at various potentials relative to ground. In experiments with K^+ as the permeant ion, symmetrical 210 mM KPIPES, pH 7.2 was used at a holding potential of −30 mV to minimise openings of SR K^+ channels, and to create a physiological Ca^{2+} ion movement of luminal to cytosolic direction. In relative permeability measurements, the luminal channel side was perfused with 210 mM $CaCl_2$, 40 mM HEPES, pH 7.2. Corrections were made for the measured liquid junction potential. Where required, a Ca^{2+} electrode (Orion 93–20; Thermo Fisher Scientific) was used to buffer Ca^{2+} to the appropriate free [Ca^{2+}] and all solutions were buffered to pH 7.2 with a Ross-type pH electrode (Orion 81–55; Thermo Ficher Scientific).

Single-channel analysis

Single-channel recordings were digitised at 20 kHz and low-pass filtered at 800 Hz or 2 kHz in experiments with Ca^{2+} or K^+ as the permeant ion, respectively. Probability of opening (Po) was determined over 3 min of continuous recording using 50% threshold analysis (Colquhoun & Sigworth, 1995) in Clampfit (Molecular Devices, USA). The Po values indicated above the representative traces shown in the figures were calculated from the full 3 min recording for that channel. Where >1 channel (N) incorporated into the bilayer, Po is reported as average Po as indicated in the equation below:

$$avgPo = \frac{NPo}{N} = \frac{Po_1 + 2Po_2 + 3Po_3 + \cdots nPo_n}{N}$$

Where only a single channel incorporated into the bilayer, lifetime analysis was performed using Clampfit. With Ca^{2+} as the permeant ion, events shorter than 1 ms were not fully resolved and were stripped from the idealisation. Lifetime distributions were fitted to a probability density function (pdf) by the method of maximum likelihood fitting (Colquhoun & Sigworth, 1995) as described previously (Sitsapesan & Williams, 1990). To estimate Po populations and identify peaks, kernel density estimations (KDE) were calculated in MatLab 2018 using a bandwidth of 0.07 (Hill, 1985). For burst analysis, the interval between bursts was defined according to the method of Magleby and Pallotta (1983) (Magleby & Pallotta, 1983). The Mann-Whitney U test was used to compare burst parameters as the number of events in a burst are described by geometric distributions (Colquhoun & Hawkes, 1981). Single events were considered as part of a burst initially but were also subsequently separated into their own group in order to compare bursts with one or more than one event.

Western blots of RyR2

50 μg of protein from mixed membrane preparations were suspended in Laemmli buffer. Samples were resolved on a 6% reducing SDS polyacrylamide gel and transferred to nitrocellulose membrane in transfer buffer with 10% methanol. Membranes were blocked for 1 h at room temperature in 5% low-fat milk in Tris-buffered saline and 0.1% Tween-20 (TBS-T). Primary antibody for RyR2 was incubated overnight at 4°C (34C, Abcam, 1:1000 dilution). Membranes were washed with TBS-T and incubated for 1 h with anti-mouse HRP-conjugated secondary antibody (GE Healthcare Lifesciences). Antibody-antigen complexes were visualised by Pierce™ enhanced chemiluminescent substrate with a Bio-Rad ChemiDoc™ Imaging System. For loading control, total protein was quantified per lane with a Coomassie stain. Densities of protein were quantified on ImageLab 6.1 software.

Statistical analysis

For each intervention, data were collected using at least 3 membrane preparations. Statistical analyses were carried out using GraphPad Prism 8 or MatLab 2018. Data were expressed as the mean ± SD and $n \geq 5$ unless otherwise stated. A p value of < 0.05 was considered statistically significant. To compare two groups, an unpaired t-test was used. A two-way ANOVA was used to compare the mean differences between groups that were split into two independent variables (e.g. genotype or $[Ca^{2+}]$). The p value for the main effect and the interaction is described in each figure legend. Where an interaction was found to be significant, the p value for the post-hoc multiple comparisons with Sidak's correction was indicated on the graph above the relevant point to compare the two genotypes. Where all individual points could not be shown on the figure, the data is included as supporting information.

Molecular modelling

Homology modelling of the HD1 domain of RyR2 was performed using MODELLER (Šali & Blundell, 1993) through the Chimera (UCSF) software (Pettersen *et al.*, 2004). The

amino acid sequences of pig and human RyR2 were obtained and extracted from RCSB PDB (Berman *et al.*, 2000) and UniProt (The UniProt Consortium, 2017) (PDB ID: 5GOA; UniProt entry: Q92736), respectively, and residues corresponding to human residues 2111–2679 (the HD1 domain, 2112–2680 in pig numbering) were used for further modelling. The HD1 domains of two WT pig RyR2 structures, open and closed states (PDB ID: 5GOA and 5GO9 (Peng *et al.*, 2016); chain A in both cases), were used as templates for the modelling. Using Chimera, small molecules were deleted from the template files. PDB files of just the HD1 of chain A were saved, followed by alignment of the sequences of HD1 for pig, human WT as well as human with either of the two mutations. Homology models were generated using the default parameters for MODELLER in Chimera except that 50 models were generated for each round of modelling and that the "thorough optimisation" procedure was applied. The resulting HD1 homology models included a total of 300 structural models of six different constructs: human WT, the V2475F mutant and the R2474S mutant, each modelled on both open and closed state pRyR2 template structures. Two lobes were defined for HD1; lobe A (residues 2111–2473) and lobe B (residues 2476–2679), and these lobes were connected by the mutation sites. The angle between these lobes was calculated by defining two vectors, both originating from centre of mass of the mutation site with one of them going to the centre of mass of lobe A and the other one to the centre of mass of lobe B. The angle between these vectors is considered the hinge angle. One-way ANOVA with Fisher's LSD test was used to compare the calculated hinge angles between the different constructs.

Materials

All chemicals were purchased from VWR or Sigma or as otherwise stated. All solutions were prepared in deionised water and filtered through a 0.45 μM pore diameter filter (Millipore).

Results

Single-channel recordings

Typical single-channel recordings of native RyR2 channels derived from the hearts of WT or V2475F(+/−) mice are shown in Fig. 2A, illustrating the similar fast gating kinetics and absence of resolvable sub-conductance state gating. The V2475F mutation produced a small but significant reduction in single-channel conductance when Ca^{2+} was the permeant ion as shown in Fig. 2B (Note that in (A), recordings from WT and V2475F(+/−) channels of similar conductance were used to aid comparison of gating behaviour). In contrast, no deviation in K^+ conductance was observed (698.4 ± 49.2 pS; n = 7 and 703.0 ± 58.6 pS; n = 8; SD in symmetrical 210 mM K^+ for WT and V2475F(+/−) channels, respectively). Under bi-ionic conditions with cytosolic 210 mM K^+ and luminal 210 mM Ca^{2+}, we also found no difference in reversal potential (see Fig. 2C), indicating that the mutation does not alter the relative Ca^{2+}: K^+ permeability ratio (PCa^{2+}/PK^+) which was 7.13 ± 0.67 and 7.15 ± 1.39 (mean ± SD; n = 5 and n = 7) for WT and V2475F(+/−) channels, respectively.

Loaiza *et al.* 2013 reported that purified recombinant V2475F(+/+) channels are more sensitive to cytosolic Ca^{2+} than WT channels. However, they suggest that there is wide

variability in gating when native channels, derived from the hearts of V2475F(+/−) mice, are incorporated into bilayers (Loaiza *et al.*, 2013). It is essential to investigate this variability because V2475F CPVT1 patients are heterozygous for the mutation, expressing both WT and mutated subunits. Hence, the RyR2 tetramers of V2475 CPVT1 patients will be constructed from varying numbers of mutated monomers, combined with WT monomers (Fig. 1). We have therefore compared the cytosolic Ca^{2+} sensitivity of native cardiac RyR2 channels from WT and V2475F(+/−) mice. Fig. 2A compares the characteristic gating responses of WT and V2475F(+/−) channels to key cytosolic [Ca^{2+}]. Most channels in both groups are completely closed (Po = 0) at diastolic free [Ca^{2+}] (100 nM) as shown in the top traces. Importantly, 14−20% of the channels do open and we illustrate the gating properties of this critical subset of channels in subsequent figures. For V2475F(+/−) RyR2, the maximum increase in Po for the total population of channels occurs at approximately 1 μM Ca^{2+} (middle traces) and channels are almost fully inactivated by 1 mM (bottom traces). The full [Ca^{2+}]-Po relationship highlights these important alterations (Fig. 3A). While the V2475F(+/−) channels are opened more readily by the increase in cytosolic [Ca^{2+}] from 100 nM to 1 μM (EC_{50} values are 0.82 μM for WT and 0.12 μM for V2475F(+/−)), they are also more readily inactivated (IC_{50} values are 5.18 mM for WT and 0.27 mM for V2475F(+/−)). It is significant that although the V2475F(+/−) channels appear to be more sensitive to cytosolic Ca^{2+}, the average peak Po that the total V2475F(+/−) channel population achieves is no higher than that of WT channels. Thus, if the overall population of V2475F(+/−) channels is considered, cytosolic Ca^{2+} appears to remain a partial agonist for this mutant RyR2.

As shown earlier in the top traces of Fig. 2A, at 100 nM Ca^{2+}, most WT (86%; n = 115) and mutant (80%; n = 95) channels are silent (Fig. 3B) (although the presence of channels in the bilayer at 100 nM Ca^{2+} was confirmed because they open when cytosolic [Ca^{2+}] is raised). However, the V2475F(+/−) channels that do open at 100 nM Ca^{2+}, exhibit significantly higher Po than that of WT channels (Fig. 3C). Representative single channel recordings (Fig. 3D) unmistakably demonstrate the typically longer openings of the V2475F(+/−) channels. Lifetime analysis provides further insight into this altered gating behaviour of mutant channels, however, only experiments where a single channel was present in the bilayer could be used for this analysis. The mean open times were significantly longer in V2475F(+/−) channels (26.63 ± 24.52 ms, n = 13, SD) than WT channels (10.64 ± 6.73 ms, n = 12, SD, p = 0.0021). The open and closed lifetime distributions for a typical WT and V2475F(+/−) channel are shown in Fig. 4A. The open lifetime distributions of WT channels at this low free [Ca^{2+}] were always best described by one or two short time constants. In contrast, the distribution of openings of V2475F(+/−) channels was shifted such that there was a greater proportion of longer events, and the best fit to the data required at least three (as in Fig. 4A) and sometimes four time constants. The closed lifetime distributions of both WT and V2475F(+/−) channels were more variable and dependent on Po (as previously described for cytosolic Ca^{2+}-regulated gating of RyR2 (Sitsapesan & Williams, 1994b)) and could usually be best described by three time constants (Fig. 4A, right). A large proportion of the V2475F(+/−) channel closings occurred to the shortest time constant, close to the minimum resolvable event duration. Looking back at the single channel recordings (Fig. 3D), it appears that these very short closings occur within bursts of openings. We therefore

performed burst analysis and the key findings are summarised in Fig. 4B and Table 1. What was especially interesting was that the interburst interval was similar for WT and V2475F(+/−) channels (left bar chart), whereas there was a 6.15-fold elongation of burst duration (middle bar chart) in V2475F(+/−) channels. Those bursts with >1 openings were 6.14 times longer in V2475F(+/−) channels compared to WT channels (right bar chart). Importantly, the fact that the interburst interval was similar in WT and V2475F(+/−) channels suggests, that while Ca^{2+} must bind to the closed channel state in both WT and mutant channels to drive channel openings, the higher Po of the V2475F(+/−) channels at 100 nM Ca^{2+} is not primarily due to greater affinity of Ca^{2+} for V2475F(+/−) channel closed states compared to WT channel closed states. Instead, the main difference between V2475F(+/−) and WT channel gating at 100 nM Ca^{2+}, is that openings are longer in V2475F(+/−) channels, suggesting that the affinity of Ca^{2+} for the open state is increased.

We then compared how mean open and closed times changed as cytosolic Ca^{2+} was increased from 100 nM for WT and V2475F(+/−) channels (Fig. 5A and B). For both WT and V2475F(+/−) channels, the main mechanism for the increase in Po at 1 μM Ca^{2+} was an increase in the frequency of channel opening as shown by the massive decrease in mean closed times. In V2475F(+/−) channels, this was more pronounced with a 208-fold decrease in comparison to the 136-fold decrease for WT channels (note that the very brief closings in V2475F(+/−) channels at 100 nM Ca^{2+} occur within the bursts). Ca^{2+} activation was not associated with increases in mean open time. Instead, as Fig. 5A demonstrates, the trend was for reductions in mean open time with increasing [Ca^{2+}]. This trend was more obvious for V2475F(+/−) channels than for WT channels. Thus, the longest open times were observed at 100 nM Ca^{2+}, and V2475F(+/−) channels were characterised by significantly longer openings than WT channels at this [Ca^{2+}] as described in the previous paragraph.

As for 100 nM Ca^{2+} (Fig. 4A), we performed lifetime analysis across the range of [Ca^{2+}] for all experiments where just a single channel was present in the bilayer. The pdfs that best fit the open and closed lifetime distributions were calculated for each channel, and the mean values for the open and closed time constants and percentage areas are shown in Fig. 5C, D, E and F. The trends for decreasing open time constants with increasing cytosolic [Ca^{2+}] can be clearly seen for both WT and V2475F(+/−) channels (Fig. 5C) and the two shortest open time constants (1 and 2) are similar for WT and V2475F(+/−) channels. 1 μM Ca^{2+} gives the peak Po for V2475F(+/−) channels with the channels still gating into the long third and fourth open states. In contrast, Po does not peak for WT channels until cytosolic Ca^{2+} is in the 10–100 μM range and, again, the WT channels also gate into the longer third and fourth open states. Thus, these longer open states appear to be important for enabling the channels to open with maximum effectiveness. Comparison of the closed lifetime distributions (Fig. 5E and F) shows that as Ca^{2+} is raised from 100 nM to 1 μM, the time constants get shorter for both WT and mutant channels (Fig. 5E) but additionally, mutant channels only transition between the two shortest closed states (time constants 1 and 2) whereas WT channels can still enter into the longer third closed state (time constant 3). Fig. 5F demonstrates that at 1 μM Ca^{2+}, 95% of closings in mutant channels are to the shortest closed state whereas in WT channels, only approximately 80% of closings are to the shortest closed state (Fig. 5F). This greater increase in frequency of opening of the mutant channels is the major factor contributing to their higher Po at 1 μM Ca^{2+} (note the log y-axis scale for open (Fig. 5C)

and closed (Fig. 5E) lifetime constants as open lifetime constants do not change by the same magnitude). These gating changes cause V2475F(+/−) channels to transition rapidly between open and closed states at peak Po levels when the cytosolic [Ca^{2+}] is 1 μM, as can be seen in the representative trace in Fig. 2A.

Fig. 3A also highlights that Ca^{2+}-inactivation is greatly affected by the V2457F mutation, causing a 19-fold increase in affinity of Ca^{2+} for inactivation sites evidenced by the shift in IC_{50} from 5.18 mM for WT to 269 μM for V2475F(+/−) channels.

Fig. 5A & B demonstrates that for V2475F(+/−) channels, mean open time decreases when cytosolic Ca^{2+} is raised above 1 μM, chiefly because the channel no longer gates into the two longest open states (Fig. 5C). The primary mechanism for inactivation, however, is the increase in the duration of closings (Fig. 5B) that clearly takes place as Ca^{2+} is raised above 10 μM. As shown in Fig. 5E and F for V2475F(+/−) channels at 1 mM Ca^{2+}, the dominance of brief closings is lost and the V2475F(+/−) channels also gate frequently into the longer closed states (time constants 2, 3 and 4). In contrast, inactivation of WT channels takes place at much higher concentrations of cytosolic Ca^{2+}. At 10 μM Ca^{2+}, the long open states (time constants 3 and 4, Fig. 5C) are still present but disappear by 1 mM Ca^{2+} when the shortest open state is the most frequently visited (>90% of openings) (Fig. 5D). Fig. 5B suggests that by 10 mM Ca^{2+}, mean closed time is starting to increase in WT channels but because the current amplitude is greatly reduced under these conditions (luminal to cytosolic driving force is reduced), the resolution of brief events is lost and so we cannot perform accurate lifetime analysis to examine this properly.

CPVT1 is a disease caused by mutations to RyR2 that manifests as an autosomal-dominant (heterozygous) disease in patients (Priori & Chen, 2011). This suggests that if all four monomers of every RyR2 molecule contained the mutation, the functional change would be too severe overall and, certainly, our V2475F(+/−) mouse model of CPVT1 is homozygous lethal (Loaiza *et al.*, 2013). The mouse model therefore mimics the human disease and our cardiac membrane preparations will contain populations of channels that have varying numbers of mutated monomers (Fig. 1). CPVT mutations can sometimes lead to a reduction in the expression levels of RyR2 protein (for example, (Zhong *et al.*, 2021)) and so we examined V2475F(+/−) RyR2 levels by immunoblot analysis (Fig. 6A and B). The V2475F mutation did not cause a reduction in RyR2 levels suggesting that all possible combinations of mutated monomers shown in Fig. 1 may be viable ion-channels. We have collected extremely large Po data sets and so we plotted Po frequency histograms for WT and V2475F(+/−) channels at the cytosolic [Ca^{2+}] of 1 μM (Fig. 6C and D). The distribution of WT channels is clearly weighted towards lower Po values which is not the case for V2475F(+/−) channels. We used the method of kernel density estimation (KDE) to highlight the possible Po populations of the WT and V2475F channels. (Fig. 6E). The main peak for WT channels data was at 0.07. For V2475F(+/−) mutated channels, the KDE suggests the presence of at least four different populations of channels identified by four peak values of 0.08, 0.34, 0.59 and 0.87. Examples of the type of gating exhibited by the V2475F(+/−) channels at these activity levels are shown in Fig. 6F. For V2475F(+/−) channels, the lowest Po component (0.08) occurs at a similar Po to that of the WT channels but three other higher Po components make up the bulk of the distribution.

RyR2 is a ligand-gated channel modulated by many soluble ligands in addition to cytosolic Ca^{2+}. To ascertain whether the mutation specifically altered cytosolic Ca^{2+} regulation of RyR2 or whether other aspects of gating were also dysfunctional, we examined the response of the channel to the three other key physiological regulators of RyR2 activity: adenine-based ligands, luminal Ca^{2+} and cytosolic Mg^{2+}. ATP was very effective at activating channels from the V2475F(+/−) mice in the presence of 1 μM cytosolic Ca^{2+} and Fig. 7A indicates the expected action of ATP. We also investigated the effects of adenosine. This ligand is less effective than ATP at activating RyR2 at the adenine nucleotide binding site because the triphosphate group is important for inducing long open states (Kermode *et al.*, 1998; Chan *et al.*, 2000; Lindsay *et al.*, 2018). However, unlike ATP, adenosine will not induce phosphorylation and does not chelate Ca^{2+}, and so is a useful test of activity that is caused purely via the RyR2 adenine nucleotide binding site. Again, as shown in Fig. 7B, adenosine activated the V2475F(+/−) channels in a manner expected for a ligand acting at the RyR2 adenine nucleotide binding site and was able to increase Po above control values by a similar increment for both WT and V2475F(+/−) channels. Compared to the increment caused by ATP, adenosine increased Po by 81% and 87% in the WT and V2475F(+/−) channels, respectively.

Luminal Ca^{2+} regulation of V2475F channels was investigated using K^+ as the permeant ion with increasing permeation by Ca^{2+} as the luminal [Ca^{2+}] was raised. Recordings were made at the holding potential of −30 mV so that current flowed in the physiological luminal to cytosolic direction. We performed the experiments in the presence of 1 μM free cytosolic Ca^{2+} and 1 mM ATP as we have previously shown that luminal Ca^{2+} alone does not activate RyR2 over physiological luminal [Ca^{2+}] and that an activator in addition to cytosolic Ca^{2+} is required for maximum response (Sitsapesan & Williams, 1994a, 1997; Lukyanenko *et al.*, 1996). Fig. 8A shows typical recordings to illustrate the potentiating effects of luminal Ca^{2+} on WT (left) and V2475F(+/−) (right) single-channel gating when Ca^{2+} is increased from 10 μM free luminal Ca^{2+} (top traces) to 1 mM free luminal Ca^{2+}. The luminal Ca^{2+}-induced increments in Po are similar to those observed with sheep cardiac RyR2 under these experimental conditions (Ching *et al.*, 2000). Fig. 8B illustrates the mean data showing the relationships between luminal [Ca^{2+}] and Po. It can be seen that while both groups of channels are stimulated by raising luminal Ca^{2+}, there is only a 2.18 fold increase in Po for V2475F(+/−) channels when luminal Ca^{2+} is raised from 10 μM Ca^{2+} to 1 mM in comparison to a 4.48-fold increase for WT channels.

The effects of the V2475F(+/−) mutation on Mg^{2+} inhibition are shown in Fig. 9. The addition of 500 μM cytosolic free Mg^{2+} to WT channels activated by 1 μM free Ca^{2+} and 1 mM adenosine, consistently decreased Po by >80%, causing reductions in both the duration and frequency of openings. This typical pronounced inhibition of WT channel gating by 500 μM cytosolic Mg^{2+} is shown in Fig. 9A (left recordings). Under identical experimental conditions, Mg^{2+} exerted a variable and much weaker inhibitory action on the gating of V2475F(+/−) channels and, as shown in Fig. 9A (right recordings), some channels could still open frequently and with long duration. The average reduction in Po for V2475F(+/−) channels was only 64%. The relationship between Po and free cytosolic [Mg^{2+}] yielded an approximate IC_{50} of 86 μM for WT channels (Fig. 9B). However, the variable effect of Mg^{2+} on V2475F(+/−) channels did not allow us to compute an accurate IC_{50} value for these

mutant channels as can be seen from the large error bars on the plotted points. On closer inspection of the individual V2475F(+/−) channel recordings, there appeared to be at least three types of response to Mg^{2+}: 1. Those channels that were inhibited by >80% (4 of 13 channels) and thus appeared similar to WT channels in their response. 2. Those channels that were inhibited by <80% (6 of 13 channels) and 3. Those channels that were activated by 500 μM or 1 mM Mg^{2+} (3 of 13 channels). Fig. 9C illustrates the mean values of Po within these groups and Fig. 9D shows representative gating of V2475F(+/−) channels within the three groups.

Alterations to the effects of cytosolic Mg^{2+} are not totally unexpected since Ca^{2+} regulation is altered and Mg^{2+} is known to compete with Ca^{2+} for both activation and inhibition sites (Meissner *et al.*, 1986; Ashley & Williams, 1990; Laver *et al.*, 1997). The affinity of Mg^{2+} for inactivation sites appears reduced, but interestingly, in a sub-population of channels, the efficacy of Mg^{2+}, once bound, is also affected. Instead of acting purely as an antagonist of RyR2, as occurs with WT channels (Fig. 9), there is a change in the interaction of Mg^{2+} with the V2475F(+/−) channels such that Mg^{2+} behaves as an agonist in 23% of experiments. The greatest proportion of V2475F(+/−) channels (46%) respond to Mg^{2+} with ‘intermediate’ inhibition and in these experiments it appears that the Mg^{2+} affinity of the channel is reduced. It is interesting that the proportion of V2475F(+/−) channels that respond to Mg^{2+} in the same manner as WT channels (i.e. ‘full’ inhibition) is 31% which is equivalent to the predicted proportion of V2475F(+/−) RyR2 tetramers that contain zero or one mutated monomer (Fig. 12B). It is therefore tempting to speculate that the degree of Mg^{2+} dysfunction is related to the number of mutated monomers such that if two monomers are mutated, then Mg^{2+} becomes less effective as an antagonist but when three or four monomers are mutated, Mg^{2+} can even induce channel activation. Overall, 69% (46% + 23%) of all V2475F(+/−) channels exhibited an altered response to Mg^{2+} which would be expected if this behaviour required the presence of two or more mutated monomers per tetramer (37.5% + 25% + 6.25% = 68.75%).

Mg^{2+} and Ca^{2+} are thought to inhibit RyR2 through common binding sites. Thus, it might be expected that Ca^{2+} inhibition of V2475F(+/−) would also be affected in the same population of channels that exhibit reduced Mg^{2+} inhibition. We therefore compared the frequency of Po values obtained in WT and V2475F(+/−) channels at 1 mM Ca^{2+} (Fig. 12Ci). It can be seen in Fig. 12Cii that whereas no WT channels (n = 10) exhibited a Po < 0.1 at 1 mM Ca^{2+}, 73% (8 of 11 channels) of V2475F(+/−) channels gated with Po < 0.1. Thus, 73% of V2475F(+/−) channels responded in an abnormal manner to 1 mM Ca^{2+}, a percentage that is very similar to the percentage of channels that respond abnormally to Mg^{2+} (68.74%), and also similar to the percentage of V2475F(+/−) RyR2 channels expected to be expressed with two or more mutated monomers (69%). This is summarised in Fig. 12B and suggests that if only one monomer is mutated, divalent cation inhibition of RyR2 is not altered.

Molecular modelling

The single point V2475F mutation caused marked functional changes despite the fact that structurally, it seems like a relatively slight change from a smaller to a larger hydrophobic sidechain. To explore whether structural models could point towards an explanation for

these changes, we constructed homology models of the RyR2 HD1 in which the mutation is found. Another CPVT1 gain-of-function mutation is located next to V2475F, namely R2474S (Lehnart *et al.*, 2008). We speculated that, given the proximity of these mutations, perhaps they would have similar structural effects, and for this reason we also constructed models of the R2474S single point mutant. Fig. 10 illustrates the locations of these mutations within HD1 of RyR2.

We used structures of the pig RyR2 in open and closed states as templates for our homology modelling (PDB ID: 5GOA, 5GO9 (Peng *et al.*, 2016) and our models were restricted to HD1 (residues 2111 to 2679). Models for human WT, human R2474S and human V2475F were constructed for both the open and the closed state. 50 models were generated for each of these six constructs, and the five best models from each group, based on their MODELLER scores, were chosen for analysis. Given the homology modelling approach applied, we did not expect major conformational changes, although the 'thorough optimization' protocol used does allow for some flexibility. However, when comparing the models, we noticed what appeared to be different hinge motions in the HD1 (Fig. 11). To analyse these differences, we defined two lobes of HD1 (Fig. 11A), linked by the mutation sites, and calculated the hinge angle between these lobes as described in the methods section. Interestingly, this hinge angle was significantly decreased for both V2475F and R2474S mutations relative to the WT models and was especially decreased when the channel was in the open state. The mean data are shown in Fig. 11B and Fig. 11C shows a cartoon illustrating the structural change.

Discussion

We find that the V2475F mutation impairs ligand regulation of RyR2 in addition to altering the Ca^{2+} ion flux through the pore. The damage to function is severe yet specific. Homology modelling proposes that these detrimental functional changes arise because of the critical location of valine 2475 at a hinge between two regions of the HD1 domain. Our HD1 models show that both the V2475F and the neighbouring CPVT1 mutation, R2474S (Jiang *et al.*, 2005; Lehnart *et al.*, 2008), reduce the angle between the two regions. From the structures of pig RyR2 in open and closed states, it has previously been suggested that the motions of the helical domain and the central domain (including the pore region) are coupled and, therefore, that shifts in the helical domain may be translated into changes in the central domain (Peng *et al.*, 2016). Thus, despite the distant location of the HD1 "hinge" region harbouring the mutation site from the affected ligand binding sites and pore region of the channel, it seems likely that the structural change proposed by our models is effectively transmitted to these regions in a manner that produces the unique alterations to conduction and gating that we observe.

By individually examining the effects of critical physiological regulators of RyR2, cytosolic and luminal Ca^{2+}, cytosolic Mg^{2+} and adenine-based ligands, we have isolated the major gating defects as specific to the interactions of cytosolic Ca^{2+} and Mg^{2+} with the channel. A decrease in single-channel Ca^{2+} conductance was evident, indicating that modifications within the conduction pathway may take place. However, there was no significant change

in K^+ conductance or in the permeability of RyR2 to Ca^{2+} relative to K^+, suggesting that alterations to SR Ca^{2+} flux during EC-coupling may be minimal.

Our results demonstrate that a particularly harmful change to the mechanism of Ca^{2+} regulation of V2475F(+/−) channels operates at the cytosolic free [Ca^{2+}] of 100 nM and we suggest that this will be key to fuelling the delayed afterdepolarisations (DADs) that are characteristic of this CPVT1 mutation (Loaiza *et al.*, 2013). Most WT (86%) and V2475F (80%) channels remain closed at 100 nM Ca^{2+}. However, the crucial mechanistic change to gating is that any V2475F(+/−) channels that open do so with much longer open times than WT channels. It is well documented that cytosolic Ca^{2+} activates normal native RyR2 channels primarily by binding to closed states of the channel to increase the frequency of opening (Ashley & Williams, 1990; Sitsapesan & Williams, 1994b). However, at 100 nM cytosolic Ca^{2+}, the main gating change to V2475F(+/−) channels is elongation of individual openings and bursts of openings rather than an increase in frequency of opening. Thus, at this low [Ca^{2+}] (100 nM), the main effect of the V2475F(+/−) mutation is not to increase the on-rate of Ca^{2+} binding to closed channel states and thereby ‘destabilise’ the closed channel state, a phrase often coined as a global description of the effects of CPVT mutations. Instead, the rate of closing is reduced in the Ca^{2+}-bound V2475F(+/−) channels causing prolonged open states.

As the [Ca^{2+}] is increased, deviation from normal Ca^{2+}-induced RyR2 gating regulation is further extended. At 1 μM Ca^{2+}, as expected, the main mechanism for the increase in Po of WT channels is the increase in frequency of channel opening. For V2475F(+/−) channels, this is also true but the effect is greater, bringing the mean closed lifetimes down to only 1.96 ± 2.18 ms (SD; n = 13) and thus causing the significantly higher overall Po at 1 μM than occurs in WT channels. The Po frequency histograms and KDEs shown in Fig. 6 demonstrate that at this [Ca^{2+}], a large proportion of the total population of RyR2 channels from WT mouse hearts have a low Po with a KDE Po peak of 0.07. In contrast, the Po values of RyR2 channels derived from V2475F(+/−) hearts fall into four distinct peaks indicating that there are at least three additional groups of channels with higher Po.

We suggest that these additional Po peaks arise due to the presence of different numbers of mutated monomers within in RyR2 tetramer. RyR2 clusters in the heart vary in size up to 100 RyR2 per cluster (Franzini-Armstrong *et al.*, 1999; Asghari *et al.*, 2020). It seems likely therefore, that Ca^{2+}-release from a cluster, especially from the larger clusters, will predominantly reflect the activity of the RyR2 channels of intermediate phenotype. Thus, those channels with either no mutated monomers or 4 mutated monomers may exert little effect overall on Ca^{2+}-release. These data highlight the necessity of using native channels from heterozygous tissue to study the effect that a CPVT1 mutation will exert in the heart.

It is noteworthy that Ca^{2+}-induced inactivation starts to kick in for V2475F(+/−) channels even at 1 μM Ca^{2+}, as evidenced by the sharp decrease in mean open times at 1 μM Ca^{2+} in addition to the gradual decrease in frequency of opening as [Ca^{2+}] further increases (whereas inactivation of WT channels only starts to be observed at approximately 1 mM). Thus, the increased affinity of Ca^{2+} for V2475F(+/−) channel inactivation sites ensures that the channel transitions only briefly to the open state. Overall, these changes in Ca^{2+}

regulation can be summed up by saying that the V2475F mutation seems to cause an intrinsic change in gating such that the open channel state is more stable at very low [Ca^{2+}] than WT channels. In addition, although the actual mechanisms by which Ca^{2+} activates and inactivates mutant channels is similar to those of WT channels, the affinity of Ca^{2+} for both activation and inactivation sites is increased.

The second major impairment to ligand regulation of V2475F(+/−) channels relates to Mg^{2+} inhibition. This is the first time, in single-channel experiments, that Mg^{2+} has been shown, not only to exhibit reduced ability to close RyR2 channels, but to behave as an agonist and activate RyR2. These changes in Mg^{2+} regulation effectively lift the brake on Ca^{2+} activation during diastole to enhance the probability of RyR2 opening to elicit DADs. For CPVT1, this is an important step forward in understanding the mechanisms driving the arrhythmic tendencies of this disease. It is notable also that the V2475F mutation is not the only CPVT1 mutation to be associated with altered Mg^{2+} regulation. Using recombinantly expressed channels, the P2328S, Q4201R, and V4653F mutations were shown to reduce the inhibitory ability of Mg^{2+} (Lehnart *et al.*, 2004) in single-channel experiments, while the R2474S and K4750Q mutations decreased the ability of Mg^{2+} to inhibit ryanodine binding (Uehara *et al.*, 2017). Regarding the R2474S mutation; as arginine2474 neighbours valine2475 within the HD1 domain, and homology modelling predicts similar structural changes when these two residues are mutated to serine or phenylalanine (Fig. 11), respectively, we would anticipate that both of these CPVT1 mutations would produce similar defects in Mg^{2+} regulation of RyR2 channels.

It has been reported that the V2475F mutation produces heightened sensitivity to the activating effects of luminal Ca^{2+} (Loaiza *et al.*, 2013), however, this was not observed in the current experiments. Both our WT and V2475F(+/−) channels were highly sensitive to micromolar concentrations of luminal Ca^{2+}, exhibiting sensitivity similar to that of native channels from sheep hearts (Sitsapesan & Williams, 1997; Ching *et al.*, 2000). In contrast, Loaiza et al. (2013) found that WT channels were not stimulated by luminal Ca^{2+} until concentrations exceeding 1 mM were reached (Loaiza *et al.*, 2013). Our different observations could be due to ATP being additionally present in our experiments as we have previously shown that the potentiating effects of luminal Ca^{2+} are minimal in the absence of another activating agent apart from cytosolic Ca^{2+} (Sitsapesan & Williams, 1994a). The reduced sensitivity to luminal Ca^{2+} could also be due to the fact that Loaiza et al. (2013) used recombinant channels for these experiments. Since use of recombinant channels ensures that all monomers of all RyR2 tetramers contain the mutation, the data provide information concerning only 6.25% of channels expressed in V2475F(+/−) hearts and these channels are likely to represent the most extreme deviation from normal function. We therefore suggest that the response of V2475F(+/−) channels to luminal Ca^{2+} that we observed, over the range of luminal [Ca^{2+}] likely to occur physiologically during the diastolic and systolic phases of the cardiac cycle, may be more representative of the changes that operate in the hearts of patients with CPVT1.

Our study highlights the need to characterise the function of native RyR2 channels derived from cardiac muscle in order to understand the phenotype of CPVT1 that emerges in patients due to the heterozygous nature of this disease. We have demonstrated significant differences

between the function of recombinantly-expressed channels described previously (Loaiza *et al.*, 2013), where every RyR2 tetramer harbours the single-point mutation in every monomer, and that of native cardiac RyR2 channels where binomial distribution predicts that only 1 in 16 RyR2 channels expressed in the heart will contain four mutated monomers. In fact, there could be even fewer than this if the mutation affects oligomerisation, membrane trafficking or the structural stability of the tetrameric protein. In agreement with our current work, Loaiza et al. (2013) noted the variable nature of gating when RyR2 from the hearts of V2475F(+/−) mice were incorporated into bilayers. In another study, Li & Chen (2001) found that heterologous co-expression of WT and CPVT1-E3987A mutated channels gave rise to channels with Po values intermediate to those of purely WT or E3987A mutated channels (Li & Chen, 2001). A necessary drawback of our experiments is that we have removed the RyR2 channels from their cellular milieu and so the combined changing influences of every interacting protein and post-translational modification is absent. Thus, the total cellular CPVT1 phenotype cannot be represented in the bilayer chamber. However, by isolating RyR2 channels in a bilayer, we have been able to exactly control the biochemical and ionic environment of the channels so that, step-by-step, we have examined the response of the channel to specific ligands in a bimolecular fashion, something that is impossible in a cell. Our results already provide information that is helpful for understanding why this particular RyR2 mutation leads to CPVT1 but they will also provide a framework for future work examining the effects of other changes to RyR2 that can happen in CPVT such as phosphorylation or the loss/gain of a binding protein.

In summary, our homology models propose that the CPVT1-V2475F mutation causes structural deformation to the HD1 domain due to the position of the mutation at the hinge region. HD1 has been suggested to be capable of transmitting signals to distant regions of the channel (Peng *et al.*, 2016) and this is confirmed by our experiments, demonstrating that highly specific changes in gating and ion conduction result from the V2475F mutation. We suggest that these gating changes would destabilise normal mechanisms of EC-coupling and increase episodes of excess SR Ca^{2+} leak to induce life-threatening arrhythmias in the manner suggested in Fig. 13. Briefly, in a V2475F CVPT1 patient who is not experiencing physical or emotional stress (Fig. 13A), our data predicts that there will be few cardiac RyR2 channels opening (20%) during diastole when free cytosolic Ca^{2+} is 100 nM (Fig. 3B) and that those openings will occur with low frequency as in people without CPVT1. The diastolic RyR2 openings will be of longer duration (Fig. 3D) in V2475F CPVT1 patients but the resultant increase in SR Ca^{2+} release may be transient (Kashimura *et al.*, 2010) as more Ca^{2+} is extruded from the cell and SR content lowered. These important mechanisms compensating for changes in RyR2 Po (Díaz *et al.*, 2005) enable net SR Ca^{2+} release to fall towards normal levels, thus preventing the generation of DADs.

The situation is different during periods of adrenergic stress (Fig. 13B) because phosphorylation of phospholamban stimulates sarcoendoplasmic reticulum Ca^{2+} ATP-ase (SERCA) activity (Tada *et al.*, 1974) leading to increased SR Ca^{2+} content (Kashimura *et al.*, 2010). The increased $[Ca^{2+}]$ in the SR increases not only the Po of RyR2 (Sitsapesan & Williams, 1994a, 1997; Lukyanenko *et al.*, 1996) but will also increase the Ca^{2+} current (Tinker *et al.*, 1993) through each open channel. In physiological conditions, the amount of Ca^{2+}-induced- Ca^{2+} released during EC-coupling is related to the amount of Ca^{2+} entering

the cell during the action potential and the SR Ca^{2+} content (Bassani *et al.*, 1995). The sensitivity of RyR2 to cytosolic activators is such that during diastole, when cytosolic Ca^{2+} falls to low levels, the openings of RyR2 are brief and rare and the SERCA-driven increase in SR Ca^{2+} content does not potentiate channel activity to the extent required to elicit DADs. In contrast to this normal physiological regulation of RyR2, Figs. 3 & 9 demonstrate the pathological changes to RyR2 gating that occur in channels derived from V2475F(+/−) hearts. Not only do V2475F(+/−) channels gate into longer open states at 100 nM Ca^{2+} (Fig. 3D), but they are also extremely sensitive to slight increases in cytosolic Ca^{2+} (EC_{50} = 120 nM) (Fig. 3A) and are not inhibited effectively by cytosolic Mg^{2+} (Fig. 9). As suggested in Fig. 13, this increased sensitivity of RyR2 to cytosolic activators is likely to be potentiated by the adrenergic-induced increase in SR [Ca^{2+}], so that Ca^{2+} waves and DADs result. Where more Ca^{2+} is released from the SR in cardiac cells from V2475F(+/−) hearts than in cells from WT hearts, the SR content might be expected to be lower after adrenergic stimulation. However, Loaiza et al. (2013) did not find evidence for this (Fig. 6C). SERCA was still able to compensate for the increase leak and SR content was not lowered below the threshold required for spontaneous Ca^{2+} release events.

Our study has exposed a number of mutation-driven changes to RyR2 function that were unexpected given the general current understanding of CPVT1. As CPVT1 can result from many different RyR2 mutations, determining the molecular changes to RyR2 ion-channel behaviour as we have done, provides the first step towards specialised treatments for patients with this severe cardiac disease.

Supplementary Material

Refer to Web version on PubMed Central for supplementary material.

Funding:

British Heart Foundation (BHF): Abigail D Wilson, BHF-FS/16/59/32735; NIH: Héctor H Valdivia, Carmen R Valdivia, R01-HL055438; NIH: Héctor H Valdivia, Carmen R Valdivia, R01-HL134344; British Heart Foundation (BHF): Charalampos Sigalas, PG/19/67/34607; Blaschko Trust: Charalampos Sigalas, N/A

Funding

A.D.W was supported by the BHF studentship BHF-FS/16/59/32735

H.H.V. and C.R.V. were supported by NIH grants R01-HL055438 and R01-HL134344

C.S. was supported by the Blaschko Trust and BHF Project Grant PG/19/67/34607

Data Availability Statement

All data is included in figures apart from Fig 3A and Fig 5C–F in which the entire raw data set is included in the Supporting Information file.

References

Alvarado FJ, Martijn Bos J, Yuchi Z, Valdivia CR, Hernández JJ, Zhao YT, Henderlong DS, Chen Y, Booher TR, Marcou CA, Van Petegem F, Ackerman MJ & Valdivia HH (2019). Cardiac

hypertrophy and arrhythmia in mice induced by a mutation in ryanodine receptor 2. JCI Insight; DOI: 10.1172/jci.insight.126544.

Asghari P, Scriven DR, Ng M, Panwar P, Chou KC, van Petegem F & Moore EDW (2020). Cardiac ryanodine receptor distribution is dynamic and changed by auxiliary proteins and post-translational modification. Elife; DOI: 10.7554/eLife.51602.

Ashley RH & Williams AJ (1990). Divalent cation activation and inhibition of single calcium release channels from sheep cardiac sarcoplasmic reticulum. J Gen Physiol 95, 981–1005. [PubMed: 2163436]

Bassani JWM, Yuan W & Bers DM (1995). Fractional SR Ca release is regulated by trigger Ca and SR Ca content in cardiac myocytes. Am J Physiol - Cell Physiol; DOI: 10.1152/ajpcell.1995.268.5.c1313.

Beard NA, Sakowska MM, Dulhunty AF & Laver DR (2002). Calsequestrin is an inhibitor of skeletal muscle ryanodine receptor calcium release channels. Biophys J 82, 310–320. [PubMed: 11751318]

Berman HM, Westbrook J, Feng Z, Gilliland G, Bhat TN, Weissig H, Shindyalov IN & Bourne PE (2000). The Protein Data Bank. Nucleic Acids Res; DOI: 10.1093/nar/28.1.235.

Bers DM (2002). Cardiac excitation-contraction coupling. Nature 415, 198–205. [PubMed: 11805843]

Bhuiyan ZA, Van Den Berg MP, Van Tintelen JP, Bink-Boelkens MTE, Wiesfeld ACP, Alders M, Postma AV., Van Langen I, Mannens MMAM & Wilde AAM (2007). Expanding spectrum of human RYR2-related disease: New electrocardiographic, structural, and genetic features. Circulation; DOI: 10.1161/CIRCULATIONAHA.107.711606.

Bongianino R, Denegri M, Mazzanti A, Lodola F, Vollero A, Boncompagni S, Fasciano S, Rizzo G, Mangione D, Barbaro S, Di Fonso A, Napolitano C, Auricchio A, Protasi F & Priori SG (2017). Allele-specific silencing of mutant mRNA rescues ultrastructural and arrhythmic phenotype in mice carriers of the R4496C mutation in the ryanodine receptor gene (RYR2). Circ Res 121, 525–536. [PubMed: 28620067]

Chan WM, Welch W & Sitsapesan R (2000). Structural factors that determine the ability of adenosine and related compounds to activate the cardiac ryanodine receptor. Br J Pharmacol 130, 1618–1626. [PubMed: 10928966]

Ching LL, Williams AJ & Sitsapesan R (2000). Evidence for Ca2+ activation and inactivation sites on the luminal side of the cardiac ryanodine receptor complex. Circ Res 87, 201–206. [PubMed: 10926870]

Colquhoun D & Hawkes AG (1981). On the stochastic properties of single ion channels. Proc R Soc London - Biol Sci; DOI: 10.1098/rspb.1981.0003.

Colquhoun D & Sigworth FJ (1995). Fitting and Statistical Analysis of Single-Channel Records. In Single-Channel Recording, pp. 483–587. Springer US, Boston, MA. Available at: http://link.springer.com/10.1007/978-1-4419-1229-9_19 [Accessed August 13, 2018].

Denegri M, Bongianino R, Lodola F, Boncompagni S, De Giusti VC, E. Avelino-Cruz J, Liu N, Persampieri S, Curcio A, Esposito F, Pietrangelo L, Marty I, Villani L, Moyaho A, Baiardi P, Auricchio A, Protasi F, Napolitano C & Priori SG (2014). Single delivery of an adeno-associated viral construct to transfer the CASQ2 gene to knock-in mice affected by catecholaminergic polymorphic ventricular tachycardia is able to cure the disease from birth to advanced age. Circulation; DOI: 10.1161/CIRCULATIONAHA.113.006901.

Díaz ME, Graham HK, O'Neill SC, Trafford AW & Eisner DA (2005). The control of sarcoplasmic reticulum Ca content in cardiac muscle. Cell Calcium; DOI: 10.1016/j.ceca.2005.06.017.

El-Ajouz S, Venturi E, Witschas K, Beech M, Wilson AD, Lindsay C, Eberhardt D, O'Brien F, Iida T, Nishi M, Takeshima H & Sitsapesan R (2017). Dampened activity of ryanodine receptor channels in mutant skeletal muscle lacking TRIC-A. J Physiol 595, 4769–4784. [PubMed: 28387457]

Else SDN, Potts JE & Sanatani S (2012). Postexertional Supraventricular Tachycardia in Children with Catecholaminergic Polymorphic Ventricular Tachycardia. Case Reports Cardiol; DOI: 10.1155/2012/329097.

Fabiato A (1983). Calcium-induced release of calcium from the cardiac sarcoplasmic reticulum. Am J Physiol - Cell Physiol; DOI: 10.1152/ajpcell.1983.245.1.c1.

Fenwick N, Griffin G & Gauthier C (2009). The welfare of animals used in science: how the "Three Rs" ethic guides improvements. Can Vet J = La Rev Vet Can.

Franzini-Armstrong C, Protasi F & Ramesh V (1999). Shape, size, and distribution of Ca2+ release units and couplons in skeletal and cardiac muscles. Biophys J 77, 1528–1539. [PubMed: 10465763]

Grundy D (2015). Principles and standards for reporting animal experiments in The Journal of Physiology and Experimental Physiology. J Physiol; DOI: 10.1113/JP270818.

Györke I, Hester N, Jones LR & Györke S (2004). The Role of Calsequestrin, Triadin, and Junctin Conferring Cardiac Ryanodine Receptor Responsiveness to Luminal Calcium. Biophys J 86, 2121–2128. [PubMed: 15041652]

Hill PD (1985). Kernel Estimation of a Distribution Function. Commun Stat - Theory Methods 14, 605–620.

Jiang D, Wang R, Xiao B, Kong H, Hunt DJ, Choi P, Zhang L & Chen SRW (2005). Enhanced Store Overload–Induced Ca $^{2+}$ Release and Channel Sensitivity to Luminal Ca $^{2+}$ Activation Are Common Defects of RyR2 Mutations Linked to Ventricular Tachycardia and Sudden Death. Circ Res 97, 1173–1181. [PubMed: 16239587]

Kashimura T, Briston SJ, Trafford AW, Napolitano C, Priori SG, Eisner DA & Venetucci LA (2010). In the RyR2R4496C mouse model of CPVT, β-adrenergic stimulation induces ca waves by increasing SR Ca content and not by decreasing the threshold for Ca Waves. Circ Res; DOI: 10.1161/CIRCRESAHA.110.227744.

Kermode H, Williams AJ & Sitsapesan R (1998). The interactions of ATP, ADP, and inorganic phosphate with the sheep cardiac ryanodine receptor. Biophys J 74, 1296–1304. [PubMed: 9512027]

Lahat H, Pras E, Olender T, Avidan N, Ben-Asher E, Man O, Levy-Nissenbaum E, Khoury A, Lorber A, Goldman B, Lancet D & Eldar M (2001). A missense mutation in a highly conserved region of CASQ2 is associated with autosomal recessive catecholamine-induced polymorphic ventricular tachycardia in Bedouin families from Israel. Am J Hum Genet; DOI: 10.1086/324565.

Laitinen PJ, Brown KM, Piippo K, Swan H, Devaney JM, Brahmbhatt B, Donarum EA, Marino M, Tiso N, Viitasalo M, Toivonen L, Stephan DA & Kontula K (2001). Mutations of the cardiac ryanodine receptor (RyR2) gene in familial polymorphic ventricular tachycardia. Circulation 103, 485–490. [PubMed: 11157710]

Laver DR, Baynes TM & Dulhunty AF (1997). Magnesium inhibition of ryanodine-receptor calcium channels: Evidence for two independent mechanisms. J Membr Biol 156, 213–229. [PubMed: 9096063]

Lavorato M, Iyer VR, Dewight W, Cupo RR, Debattisti V, Gomez L, De La Fuente S, Zhao YT, Valdivia HH, Hajnóczky G & Franzini-Armstrong C (2017). Increased mitochondrial nanotunneling activity, induced by calcium imbalance, affects intermitochondrial matrix exchanges. Proc Natl Acad Sci U S A; DOI: 10.1073/pnas.1617788113.

Lehnart SE, Mongillo M, Bellinger A, Lindegger N, Chen BX, Hsueh W, Reiken S, Wronska A, Drew LJ, Ward CW, Lederer WJ, Kass RS, Morley G & Marks AR (2008). Leaky Ca2+ release channel/ryanodine receptor 2 causes seizures and sudden cardiac death in mice. J Clin Invest 118, 2230–2245. [PubMed: 18483626]

Lehnart SE, Wehrens XHT, Laitinen PJ, Reiken SR, Deng SX, Cheng Z, Landry DW, Kontula K, Swan H & Marks AR (2004). Sudden death in familial polymorphic ventricular tachycardia associated with calcium release channel (ryanodine receptor) leak. Circulation 109, 3208–3214. [PubMed: 15197150]

Li P & Chen SRW (2001). Molecular basis of Ca2+ activation of the mouse cardiac Ca2+ release channel (ryanodine receptor). J Gen Physiol 118, 33–44. [PubMed: 11429443]

Lindsay C, Sitsapesan M, Chan WM, Venturi E, Welch W, Musgaard M & Sitsapesan R (2018). Promiscuous attraction of ligands within the ATP binding site of RyR2 promotes diverse gating behaviour. Sci Rep 8, 1–13. [PubMed: 29311619]

Liu N, Colombi B, Memmi M, Zissimopoulos S, Rizzi N, Negri S, Imbriani M, Napolitano C, Lai FA & Priori SG (2006). Arrhythmogenesis in catecholaminergic polymorphic ventricular tachycardia: Insights from a RyR2 R4496C knock-in mouse model. Circ Res; DOI: 10.1161/01.RES.0000235869.50747.e1.

Liu Y, Kimlicka L, Hiess F, Tian X, Wang R, Zhang L, Jones PP, Van Petegem F & Wayne Chen SR (2013). The CPVT-Associated RyR2 mutation G230C enhances store overloadinduced Ca2+ release and destabilizes the N-terminal domains. Biochem J; DOI: 10.1042/BJ20130594.

Loaiza R, Benkusky NA, Powers PP, Hacker T, Noujaim S, Ackerman MJ, Jalife J & Valdivia HH (2013). Heterogeneity of ryanodine receptor dysfunction in a mouse model of catecholaminergic polymorphic ventricular tachycardia. Circ Res 112, 298–308. [PubMed: 23152493]

Lukyanenko V, Györke I & Györke S (1996). Regulation of calcium release by calcium inside the sarcoplasmic reticulum in ventricular myocytes. Pflugers Arch Eur J Physiol; DOI: 10.1007/s004240050233.

Magleby KL & Pallotta BS (1983). Burst kinetics of single calcium-activated potassium channels in cultured rat muscle. J Physiol 344, 605–623. [PubMed: 6317854]

Marx SO, Reiken S, Hisamatsu Y, Jayaraman T, Burkhoff D, Rosemblit N & Marks AR (2000). PKA phosphorylation dissociates FKBP12.6 from the calcium release channel (ryanodine receptor): Defective regulation in failing hearts. Cell 101, 365–376. [PubMed: 10830164]

Meissner G, Darling E & Eveleth J (1986). Kinetics of Rapid Ca2+ Release by Sarcoplasmic Reticulum. Effects of Ca2+, Mg2+, and Adenine Nucleotides. Biochemistry 25, 236–244. [PubMed: 3754147]

Meissner G & Henderson JS (1987). Rapid calcium release from cardiac sarcoplasmic reticulum vesicles is dependent on Ca2+ and is modulated by Mg2+, adenine nucleotide, and calmodulin. J Biol Chem; DOI: 10.1016/s0021-9258(18)61469-3.

Näbauer M, Callewaert G, Cleemann L & Morad M (1989). Regulation of calcium release is gated by calcium current, not gating charge, in cardiac myocytes. Science (80-); DOI: 10.1126/science.2543067.

Napolitano C, Priori SG & Bloise R (2016). Catecholaminergic Polymorphic Ventricular Tachycardia. In GeneReviews®. University of Washington, Seattle.

Nozaki Y, Kato Y, Uike K, Yamamura K, Kikuchi M, Yasuda M, Ohno S, Horie M, Murayama T, Kurebayashi N & Horigome H (2020). Co-phenotype of left ventricular non-compaction cardiomyopathy and atypical catecholaminergic polymorphic ventricular tachycardia in association with R169q, a ryanodine receptor type 2 missense mutation. Circ J; DOI: 10.1253/circj.CJ-19-0720.

Peng W, Shen H, Wu J, Guo W, Pan X, Wang R, Chen SRW & Yan N (2016). Structural basis for the gating mechanism of the type 2 ryanodine receptor RyR2. Science (80-); DOI: 10.1126/science.aah5324.

Pettersen EF, Goddard TD, Huang CC, Couch GS, Greenblatt DM, Meng EC & Ferrin TE (2004). UCSF Chimera - A visualization system for exploratory research and analysis. J Comput Chem 25, 1605–1612. [PubMed: 15264254]

Priori SG & Chen SRW (2011). Inherited dysfunction of sarcoplasmic reticulum Ca2+ handling and arrhythmogenesis. Circ Res 108, 871–883. [PubMed: 21454795]

Priori SG, Napolitano C, Memmi M, Colombi B, Drago F, Gasparini M, DeSimone L, Coltorti F, Bloise R, Keegan R, Cruz Filho FES, Vignati G, Benatar A & DeLogu A (2002). Clinical and molecular characterization of patients with catecholaminergic polymorphic ventricular tachycardia. Circulation 106, 69–74. [PubMed: 12093772]

Priori SG, Napolitano C, Tiso N, Memmi M, Vignati G, Bloise R, Sorrentino V & Danieli GA (2001). Mutations in the cardiac ryanodine receptor gene (hRyR2) underlie catecholaminergic polymorphic ventricular tachycardia. Circulation; DOI: 10.1161/01.CIR.103.2.196.

Roston TM, Guo W, Krahn AD, Wang R, Van Petegem F, Sanatani S, Chen SRW & Lehman A (2017). A novel RYR2 loss-of-function mutation (I4855M) is associated with left ventricular non-compaction and atypical catecholaminergic polymorphic ventricular tachycardia. J Electrocardiol; DOI: 10.1016/j.jelectrocard.2016.09.006.

Rousseau E, Smith JS, Henderson JS & Meissner G (1986). Single channel and 45Ca2+ flux measurements of the cardiac sarcoplasmic reticulum calcium channel. Biophys J; DOI: 10.1016/S0006-3495(86)83543-3.

Šali A & Blundell TL (1993). Comparative protein modelling by satisfaction of spatial restraints. J Mol Biol 234, 779–815. [PubMed: 8254673]

Sitsapesan R, Montgomery RA, MacLeod KT & Williams AJ (1991). Sheep cardiac sarcoplasmic reticulum calcium-release channels: modification of conductance and gating by temperature. J Physiol 434, 469–488. [PubMed: 1850797]

Sitsapesan R & Williams AJ (1990). Mechanisms of caffeine activation of single calcium-release channels of sheep cardiac sarcoplasmic reticulum. J Physiol; DOI: 10.1113/jphysiol.1990.sp018031.

Sitsapesan R & Williams AJ (1994a). Regulation of the gating of the sheep cardiac sarcoplasmic reticulum ca2+-release channel by luminal Ca2+. J Membr Biol 137, 215–226. [PubMed: 8182731]

Sitsapesan R & Williams AJ (1994b). Gating of the native and purified cardiac SR Ca(2+)-release channel with monovalent cations as permeant species. Biophys J 67, 1484–1494. [PubMed: 7819484]

Sitsapesan R & Williams AJ (1997). Regulation of current flow through ryanodine receptors by luminal Ca2+. J Membr Biol 159, 179–185. [PubMed: 9312207]

Swan H, Piippo K, Viitasalo M, Heikkilä P, Paavonen T, Kainulainen K, Kere J, Keto P, Kontula K & Toivonen L (1999). Arrhythmic disorder mapped to chromosome 1q42-q43 causes malignant polymorphic ventricular tachycardia in structurally normal hearts. J Am Coll Cardiol; DOI: 10.1016/S0735-1097(99)00461-1.

Tada M, Kirchberger MA, Repke DI & Katz AM (1974). The stimulation of calcium transport in cardiac sarcoplasmic reticulum by adenosine 3':5' monophosphate dependent protein kinase. J Biol Chem; DOI: 10.1016/s0021-9258(19)42237-0.

The UniProt Consortium (2017). UniProt: the universal protein knowledgebase. Nucleic Acids Res 45, D158–D169. [PubMed: 27899622]

Tinker A, Lindsay ARG & Williams AJ (1993). Cation conduction in the calcium release channel of the cardiac sarcoplasmic reticulum under physiological and pathophysiological conditions. Cardiovasc Res; DOI: 10.1093/cvr/27.10.1820.

Uehara A, Murayama T, Yasukochi M, Fill M, Horie M, Okamoto T, Matsuura Y, Uehara K, Fujimoto T, Sakurai T & Kurebayashi N (2017). Extensive Ca2+ leak through K4750Q cardiac ryanodine receptors caused by cytosolic and luminal Ca2+ hypersensitivity. J Gen Physiol; DOI: 10.1085/jgp.201611624.

Wehrens XHT, Lehnart SE, Huang F, Vest JA, Reiken SR, Mohler PJ, Sun J, Guatimosim S, Song LS, Rosemblit N, D'Armiento JM, Napolitano C, Memmi M, Priori SG, Lederer WJ & Marks AR (2003). FKBP12.6 deficiency and defective calcium release channel (ryanodine receptor) function linked to exercise-induced sudden cardiac death. Cell 113, 829–840. [PubMed: 12837242]

Xiao Z, Guo W, Sun B, Hunt DJ, Wei J, Liu Y, Wang Y, Wang R, Jones PP, Back TG & Chen SRW (2016). Enhanced Cytosolic Ca2+ Activation Underlies a Common Defect of Central Domain Cardiac Ryanodine Receptor Mutations Linked to Arrhythmias. J Biol Chem 291, 24528–24537. [PubMed: 27733687]

Zhong X, Guo W, Wei J, Tang Y, Liu Y, Zhang JZ, Tan VH, Zhang L, Wang R, Jones PP, Napolitano C, Priori SG & Wayne Chen SR (2021). Identification of loss-of-function RyR2 mutations associated with idiopathic ventricular fibrillation and sudden death. Biosci Rep; DOI: 10.1042/BSR20210209.

Key Points summary

1. RyR2 mutations can cause type-1 catecholaminergic polymorphic ventricular tachycardia (CPVT1), a lethal, autosomal-dominant arrhythmic disease. However, the changes in RyR2 ion-channel function that result from the many different patient mutations are rarely investigated in detail and often only recombinant RyR2, homozygous for the mutation, are studied. As CPVT1 is a heterozygous disease and the tetrameric RyR2 channels expressed in the heart will contain varying numbers of mutated monomers, we have investigated the range of RyR2 single-channel abnormalities found in the hearts of mice heterozygous for the CPVT1 mutation, V2475F(+/−)-RyR2.
2. Specific alterations to ligand regulation of V2475F(+/−)-RyR2 were observed. Multiple sub-populations of channels exhibited varying degrees of abnormality. In particular, an increased sensitivity to activating and inactivating cytosolic [Ca^{2+}], and reduced sensitivity to Mg^{2+} inhibition were evident.
3. Our results provide mechanistic insight into the changes to RyR2 gating that destabilise SR Ca^{2+}-release causing life-threatening arrhythmias in V2475F(+/−)-CPVT1 patients.

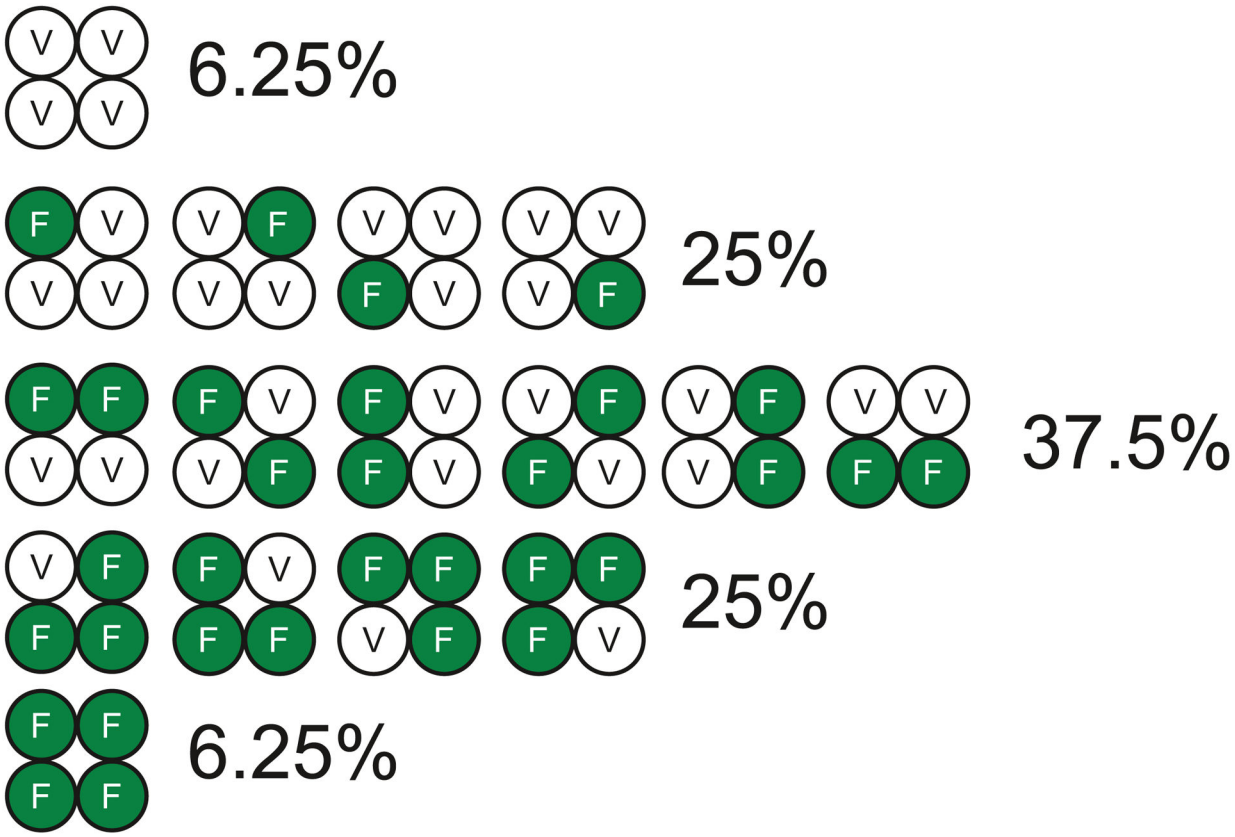

Figure 1. Likelihood of formation of RyR2 tetramers with different compositions of V2475F mutated monomers.

White (V) and green (F) circles represent WT and V2475F(+/−) mutated monomers, respectively. Assuming random assembly and identical surface expression, the probabilities of tetramers with the indicated numbers of mutant or WT subunits per tetrameric RyR2 channel is indicated as a percentage (%).

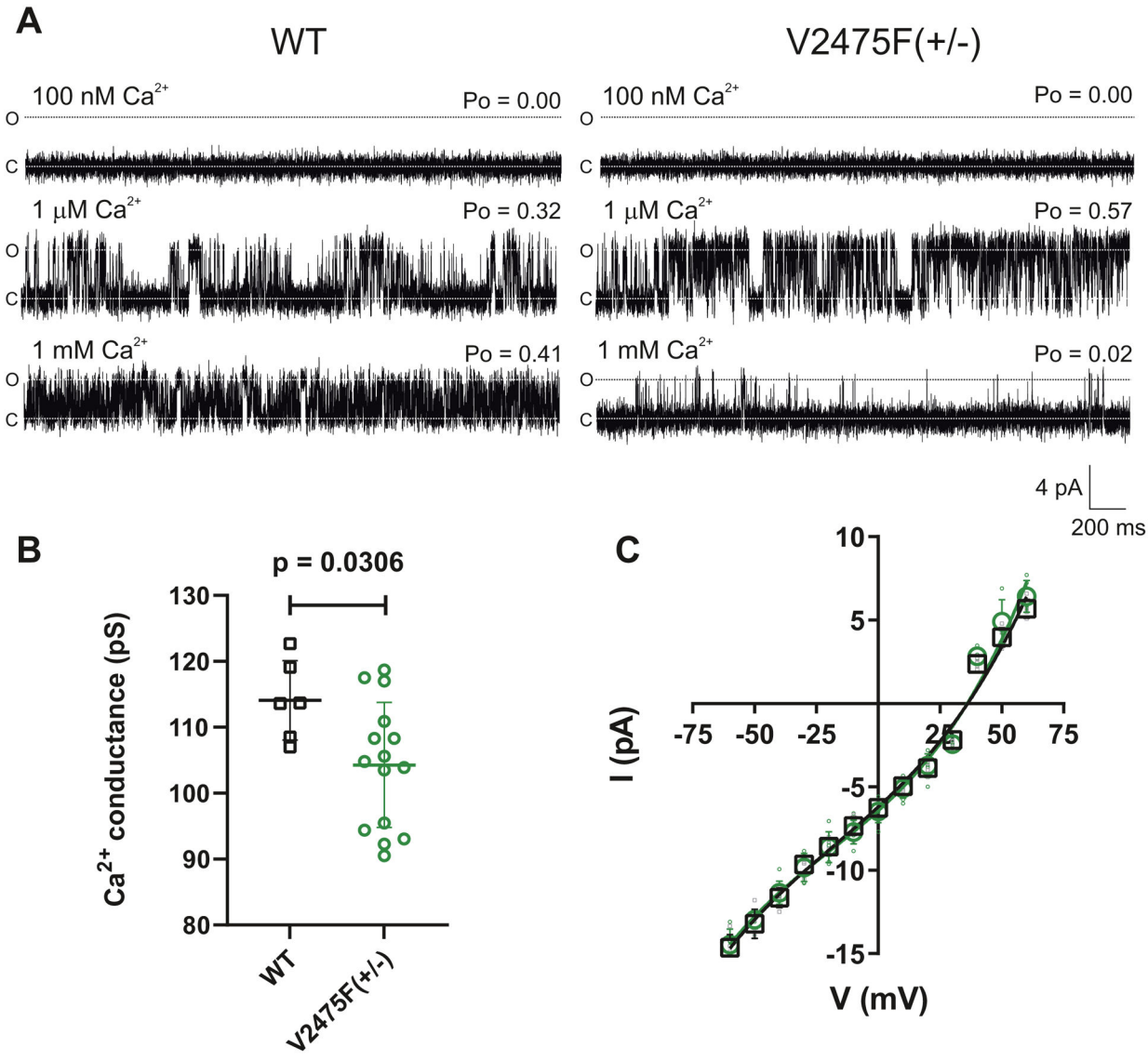

Figure 2. Typical gating and conduction properties of native RyR2 channels derived from the hearts of WT and V2475F(+/−) mice.

(A) Representative single-channel traces in Tris/HEPES, Ca^{2+} glutamate solutions (see methods), illustrating the effects of varying cytosolic [Ca^{2+}] on gating and conductance for WT (left panel) and V2475F(+/−) (right panel) channels. Luminal [Ca^{2+}] is approximately 50 mM and the cytosolic free [Ca^{2+}] is indicated above each trace along with the average Po (measured over 3 min). O and C represent the fully open and closed levels, respectively. For comparative purposes, WT and V2475F(+/−) channel traces from channels with similar single-channel conductances are shown. **(B)** Single-channel conductance of WT (black) and V2475F(+/−) (green) channels in the same solutions as in (A) with cytosolic Ca^{2+} maintained at 1 μM. Bars indicate mean ± SD; unpaired t-test, p = 0.0306. **(C)** Single-channel current-voltage relationships with luminal 210 mM K^+ and cytosolic 210 mM Ca^{2+}. Mean ± SD, n ≥ 5, for WT (black squares) and V2475F(+/−) (green circles). The third order

polynomial lines plotted for each genotype are not different, p = 0.4060. Where not shown, error bars are within the symbol.

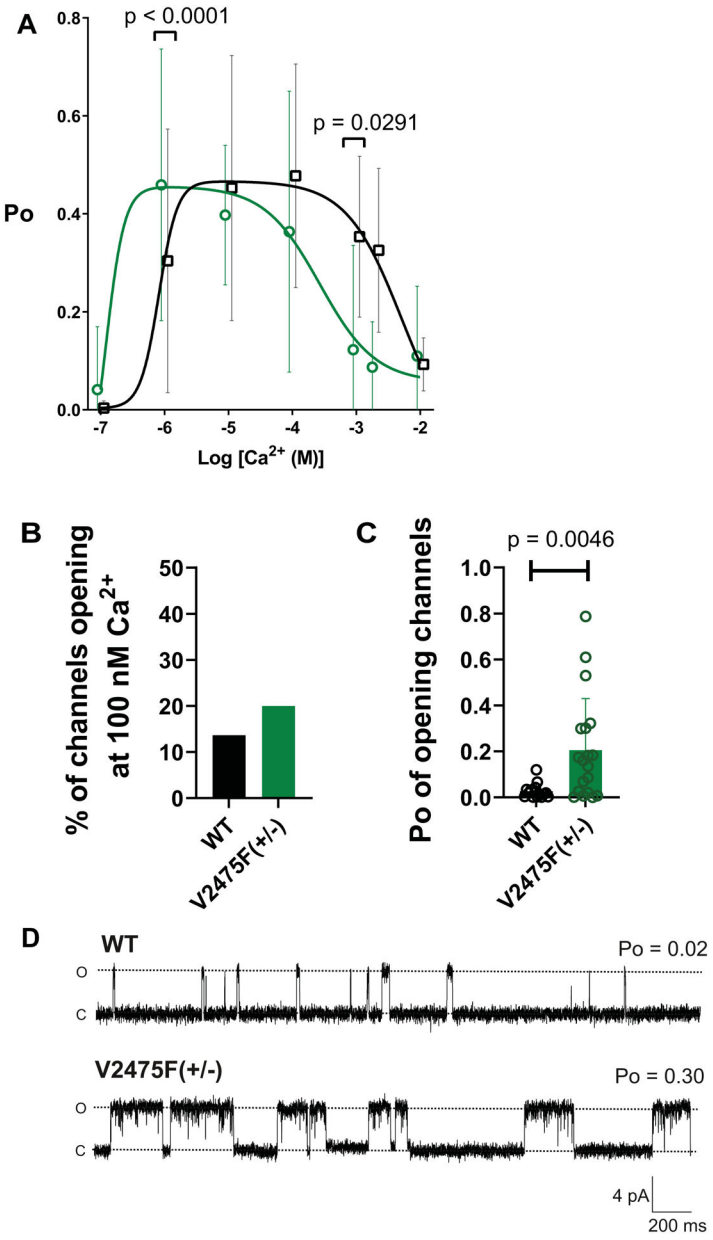

Figure 3. Effects of the V2475F mutation on the response of RyR2 channels to cytosolic Ca^{2+}.

(A) Relationship between [Ca^{2+}] and Po values for RyR2 derived from WT (black) and V2475F(+/−) (green) mice. Two-way ANOVA: Ca^{2+}-by-genotype interaction, $p < 0.0001$; main effect of Ca^{2+}, $p < 0.0001$; main effect of genotype $p = 0.0325$. Post-hoc multiple comparisons with Sidak's correction comparing WT and V2475F(+/−): $p < 0.0001$ at 1 μM, $p = 0.0291$ at 1 mM Ca^{2+}. Mean ± SD; n for WT = 8 – 110, n for VF = 5 – 95. Lines display non-linear bell-shaped fitted curves. EC_{50} values are 0.82 μM for WT and 0.12 μM for V2475F, and IC_{50} values are 5.18 mM for WT and 0.27 mM for V2475F. **(B)** Percentage of channels that open at 100 nM Ca^{2+} (n = 110 and n = 95 for WT and V2475F(+/–), respectively). **(C)** Po of single channels that open at 100 nM Ca^{2+}. Only channels that do open at 100 nM Ca^{2+} are included for WT (n = 15) and V2475F(+/–) (n = 19) mean

Po values ± SD. Unpaired t-test; p = 0.0046. **(D)** Representative recordings from WT and V2475F(+/–) mice at 100 nM cytosolic Ca^{2+}. Po displayed is for the full 3 min recording. C and O indicate the closed and open states, respectively.

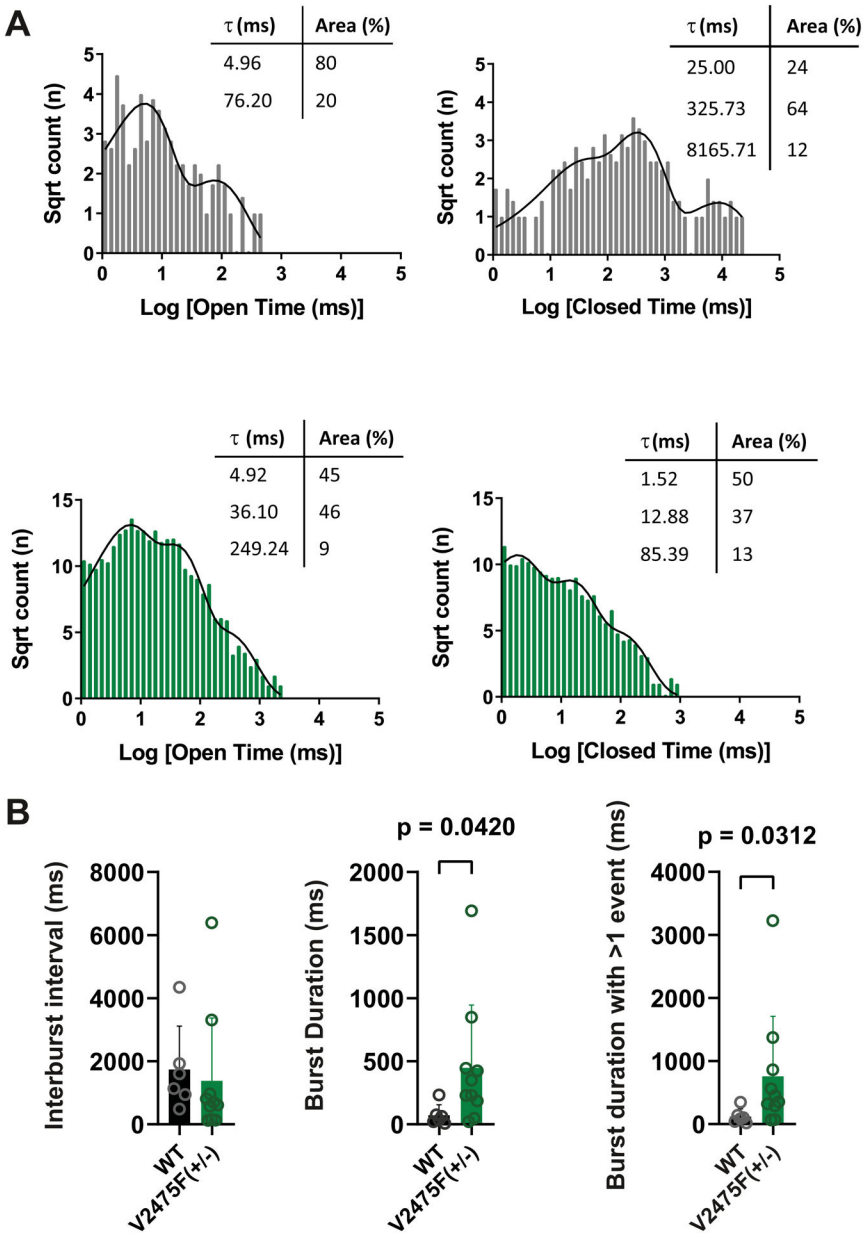

Figure 4. Effects of the V2475F mutation on the response of RyR2 channels to 100 nM cytosolic Ca^{2+}.

(A) Open and closed lifetime distributions. Open (left) and closed (right) lifetime distributions and pdfs for representative single RyR2 channels derived from WT (black) or V2475F(+/−) (green) mice in the presence of 100 nM cytosolic Ca^{2+}. The best fits to the data were obtained by the method of maximum likelihood and the resulting time constants (**τ**, ms) and percentage areas (%) are shown. **(B)** Burst analysis parameters comparing interburst interval (left, Mann-Whitney test; p = 0.1806), burst duration (middle, Mann-Whitney test; p = 0.0420), and burst duration with >1 event (right, Mann-Whitney test; p = 0.0312) for WT (black) and V2475F(+/−) (green) conducted on single channels at 100 nM cytosolic Ca^{2+}. n = 6 for WT, n = 10 for V2475F(+/−), mean ± SD.

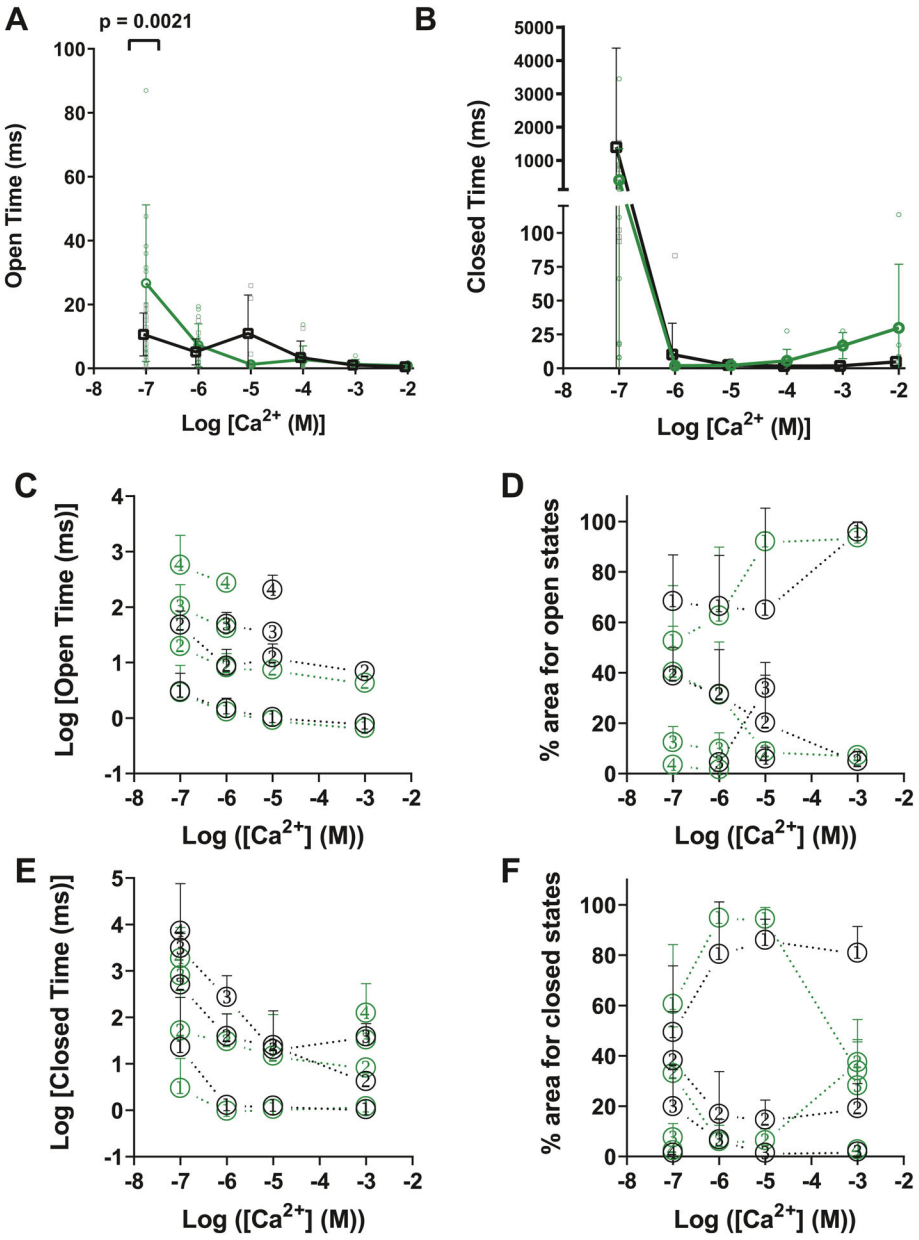

Figure 5. Effects of the V2475F mutation on open and closed lifetimes.

(A) Relationships between mean open lifetimes for WT (black) and V2475F (green). Two-way ANOVA: Ca^{2+}-by-genotype interaction, p = 0.0283; main effect of Ca^{2+}, p <0.0001; no main effect of genotype, p = 0.5733. Post-hoc multiple comparisons with Sidak's correction comparing WT and V2475F(+/−): p = 0.0021 at 100 nM. Mean ± SD, n ≥ 4. **(B)** Relationships between mean closed lifetimes for WT (black) and V2475F (green). At pCa^{2+} = 7, only channels that opened are included. Two-way ANOVA: no Ca^{2+}-by-genotype interaction, p = 0.6504; no main effect of Ca^{2+}, p = 0.0663; no main effect of genotype, p = 0.5504. Mean ± SD, n ≥ 4. **(C) – (F):** The fitting of pdfs to open and closed lifetime histograms, examples of which are shown in Fig. 4A, was performed for all experiments (where only a single channel was gating in the bilayer) across the range of cytosolic [Ca^{2+}]

shown in panels **(A)** and **(B)**. The symbols (WT = open black circles; V2475F(+/−) = open green circles) in panels **(C) – (F)** represent the mean time constants (**τ**) of the pdfs to open **(C)** and closed lifetime distributions **(E)** and their respective % areas **(D and F)**. The numbers within the symbols refer to the 1st (shortest), 2nd, 3rd and 4th time constants. To aid visualisation of the Ca^{2+}-dependent changes, the same time constants and their areas are joined with a dashed line. Where the longest time constants do not exist in every $[Ca^{2+}]$, the points are not joined with a dashed line. Mean ± SD, $n \geq 4$ (except for long open 3rd or 4th components which did not occur in all channels and where $n \geq 2$). The entire raw data set is provided in the Supporting Information.

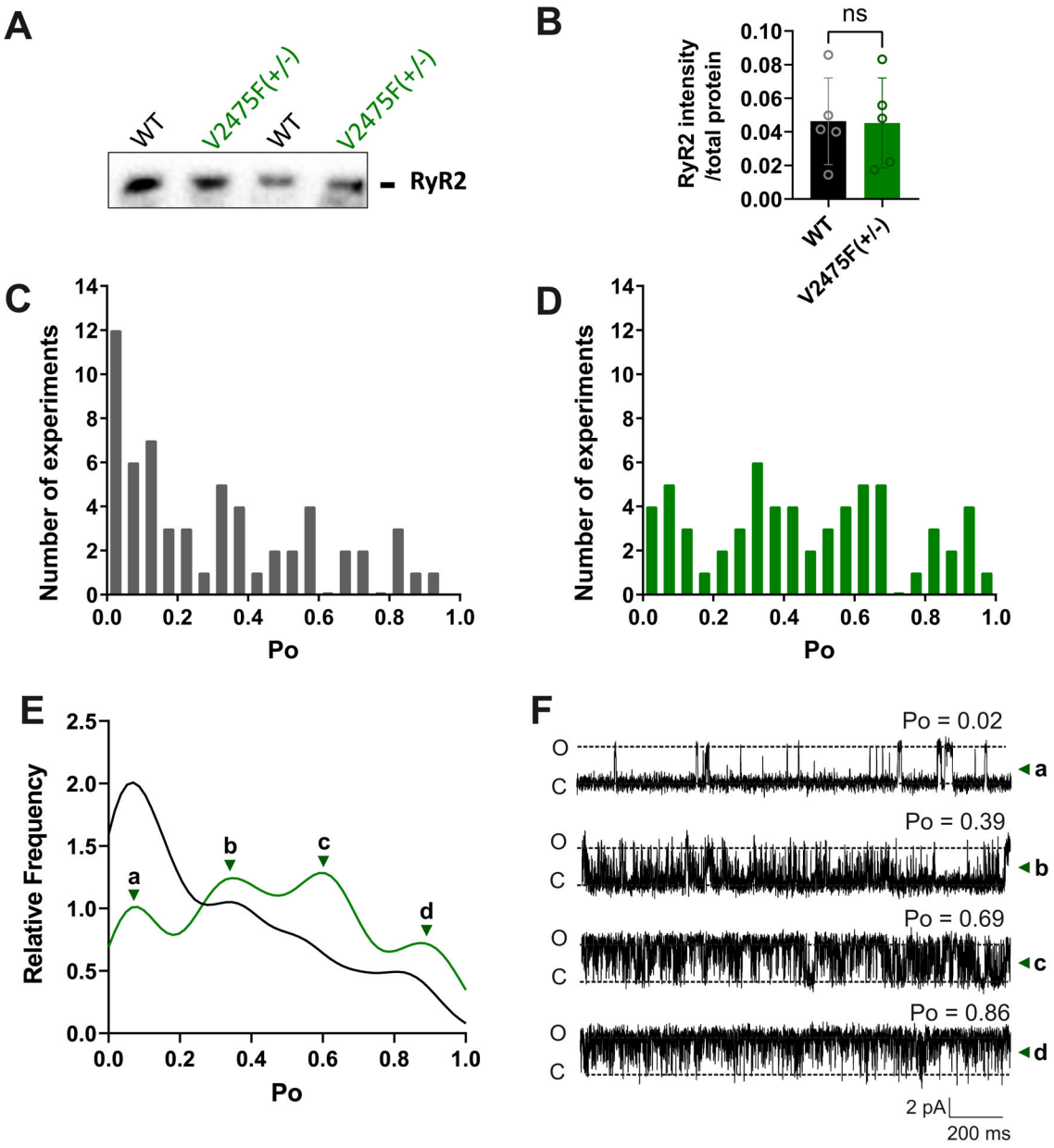

Figure 6. Effects of the V2475F mutation on expression levels of RyR2 and on the population frequency of high Po RyR2 channels in mouse cardiac muscle.

(A) Representative western blot of RyR2 derived from WT or V2475F(+/−) hearts. **(B)** Band intensity of RyR2 normalised to total protein per lane comparing RyR2 derived from WT or V2475F(+/−) hearts (mean ± SD). Each point represents a sample from an independent mixed membrane preparation (n = 5). Unpaired t-test; p = 0.9519. Po values from individual experiments were plotted as frequency distributions for **(C)** WT (n = 59) and **(D)** V2475F(+/−) (n = 62) experiments in the presence of 1 μM cytosolic Ca^{2+}. **(E)** A Kernel Density Estimate (KDE) was fit to the WT and V2475F(+/−) Po values. For the V2475F(+/−) Po values, the KDE estimated 4 peaks and therefore suggests the presence of at least four different populations of activity at Po values of 0.08, 0.34, 0.59 and 0.87. **(F)** The gating

behaviour of typical V2475F(+/−) channels drawn from these populations peaks are shown in the four traces labelled for the corresponding component.

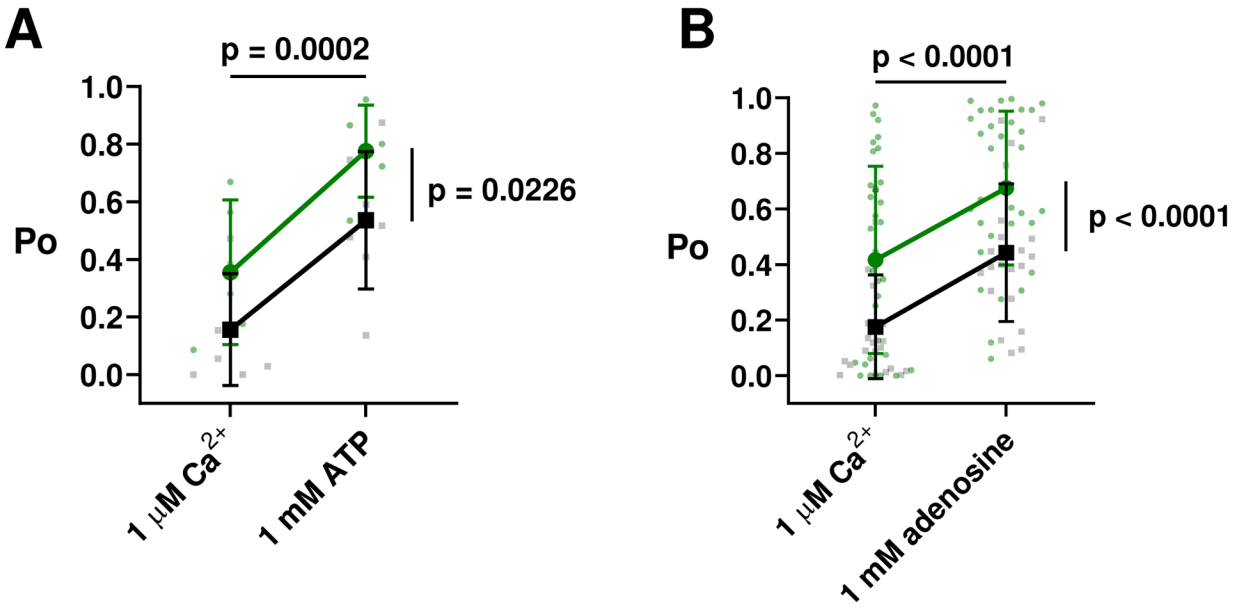

Figure 7. ATP and adenosine activation of RyR2 from WT or V2475F(+/−) mouse hearts.

(A) shows the activation of WT (black) and V2475F (green) channels by ATP. Two-way ANOVA: no ATP-by-genotype interaction, p = 0.8203; main effect of ATP, p = 0.0002; main effect of genotype, p = 0.0226. Mean ± SD, n = 7 for WT and n = 5 for V2475F. **(B)** shows the activation of WT (black) and V2475F (green) channels by adenosine. Two-way ANOVA: no adenosine-by-genotype interaction, p = 0.9379; main effect of Ca^{2+}, p < 0.0001; main effect of genotype, p < 0.0001. Mean ± SD; n = 21 for WT and n = 33 for V2475F. In both cases, control channels were activated solely by 1 μM cytosolic Ca^{2+} and the free [Ca^{2+}] was maintained at 1 μM after ATP or adenosine addition by buffering with EGTA where required.

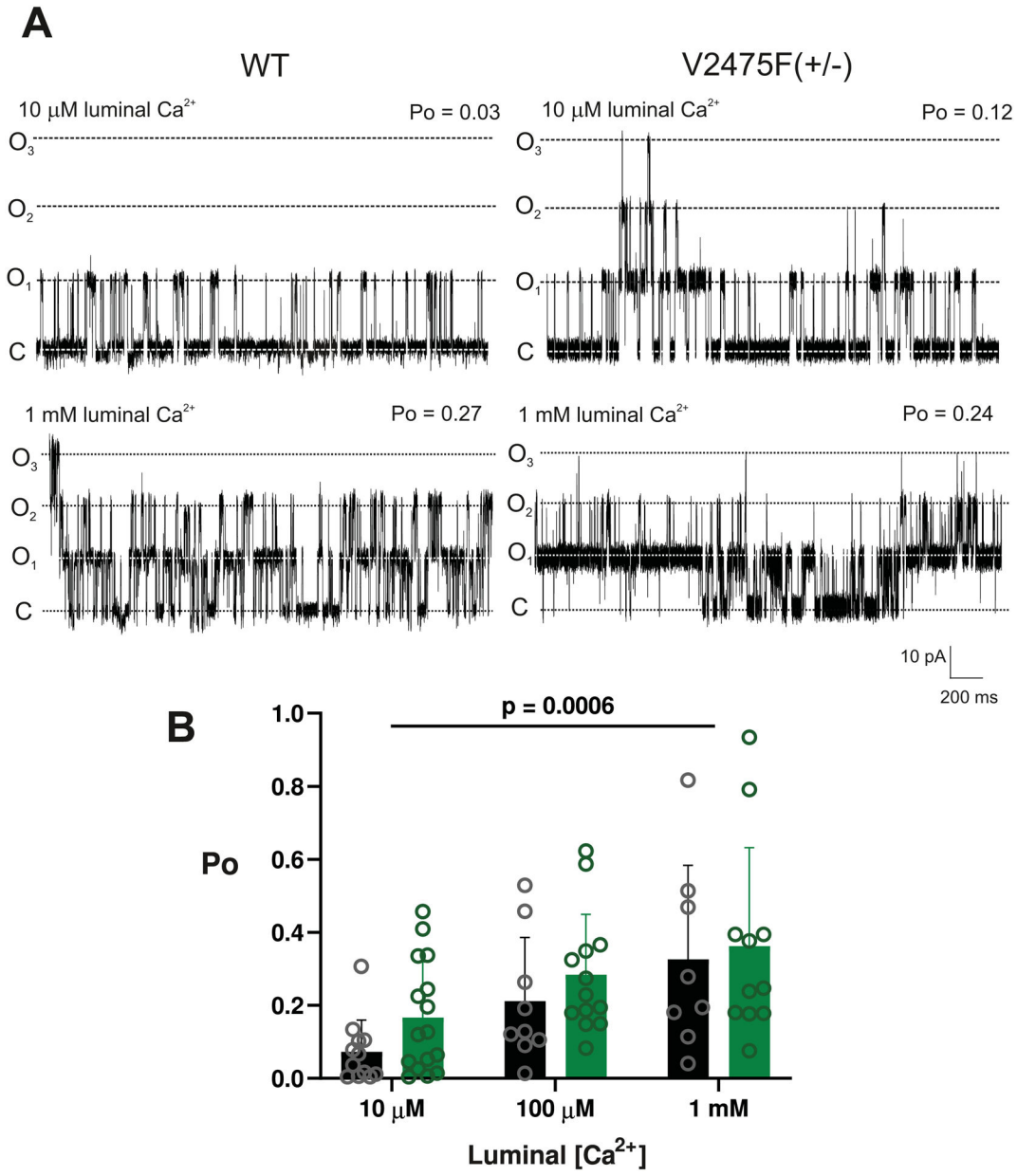

Figure 8. Luminal Ca^{2+} regulation of WT and V2475F(+/−) channel gating

(A) Representative recordings of WT and V2475F(+/−) channels in symmetrical 210 mM K^+ solutions in the presence of cytosolic activators 1 μM Ca^{2+} and 1 mM ATP at the indicated luminal [Ca^{2+}]. The holding potential was −30 mV and current flow was in the luminal to cytosolic direction. C indicates the closed channel level and O1, O2 and O3 illustrate the levels where one, two and three channels, respectively, are open. **(B)** Relationship between Po and luminal [Ca^{2+}] for WT and V2475F(+/−) channels activated by cytosolic 1 μM Ca^{2+} and 1 mM ATP. Mean ± SD, n ≥ 5. Two-way ANOVA: no Ca^{2+}-by-genotype interaction, p = 0.8766; main effect of Ca^{2+}, p = 0.0006 (indicated on the figure); no main effect of genotype p = 0.1476.

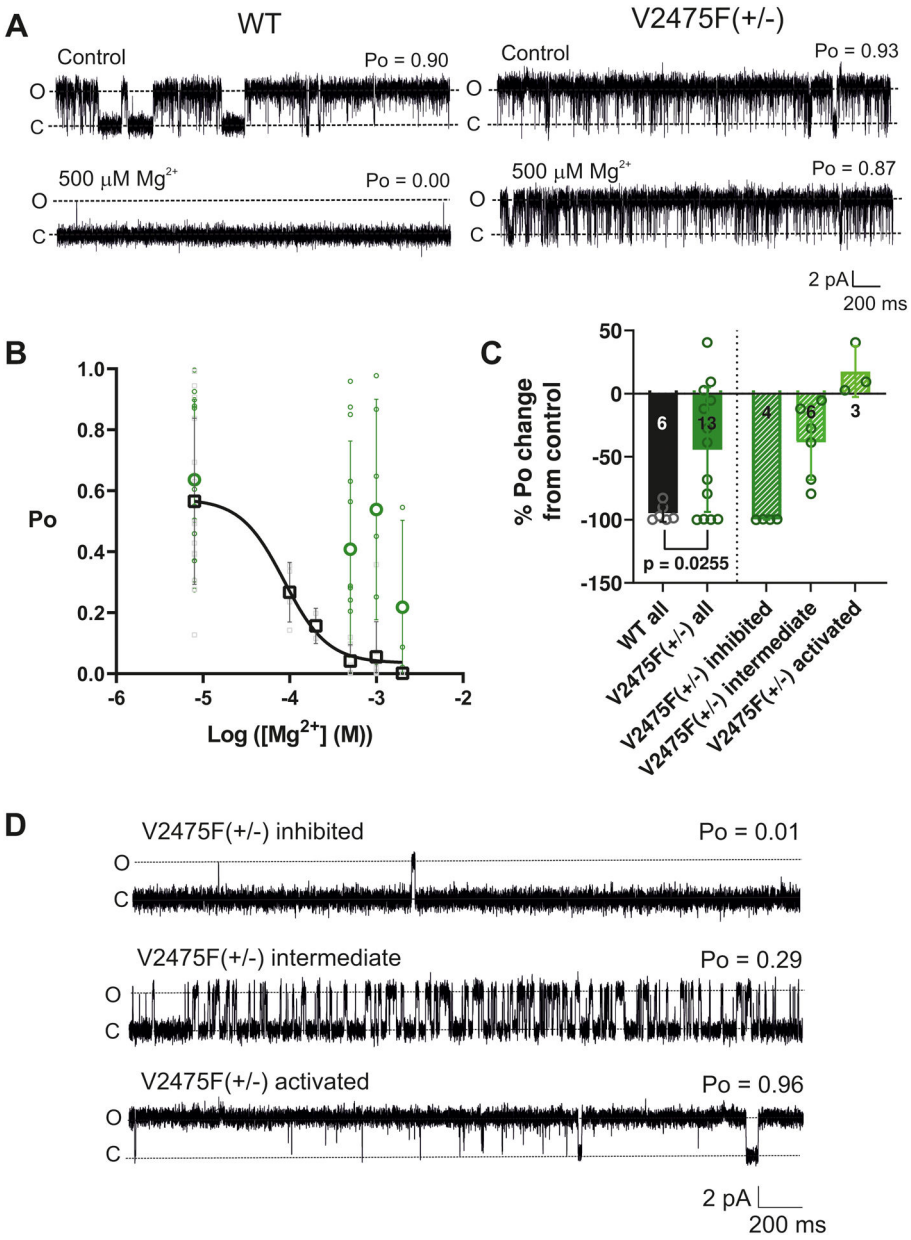

Figure 9. Effect of cytosolic Mg^{2+} on the gating of WT and V2475F channels

(A) Recordings from WT (left) and V2475F (right) channels before and after adding 500 μM free cytosolic [Mg^{2+}] in the presence of 1 mM adenosine and a maintained 1 μM free cytosolic [Ca^{2+}] (control). In order to directly compare the ability of Mg^{2+} to inhibit WT and V2475F channels, recordings from channels with a similar Po under control conditions were chosen. O and C indicate the open and closed states, respectively. **(B)** Relationship between Po and free [Mg^{2+}] for WT (black) and V2475F (green) channels in the presence of 1 μM free Ca^{2+} and 1 mM adenosine. Mean ± SD, n ≥ 5**. (C)** Left of the dashed line: comparison of the percentage inhibition of Po induced by 500 μM Mg^{2+} in all WT (black) and all V2475F (green) channels. Unpaired t-test, p = 0.0255. Right of the dashed line: percentage change in Po of V2475F channels after the channels are separated into 3

groups: those channels inhibited to within the range of inhibition expected for WT channels (>80% inhibition, n = 4), those channels inhibited to a reduced or intermediate extent (<80% inhibition, n = 6) and those channels that were activated (increase in Po, n = 3) by Mg^{2+}. Mean ± SD, n numbers for each group are indicated on the bars. **(D)** Typical examples of the gating behaviour of V2475F channels showing WT-like inhibition (top trace), intermediate inhibition (middle trace) and activation (bottom trace) in response to 500 μM Mg^{2+}.

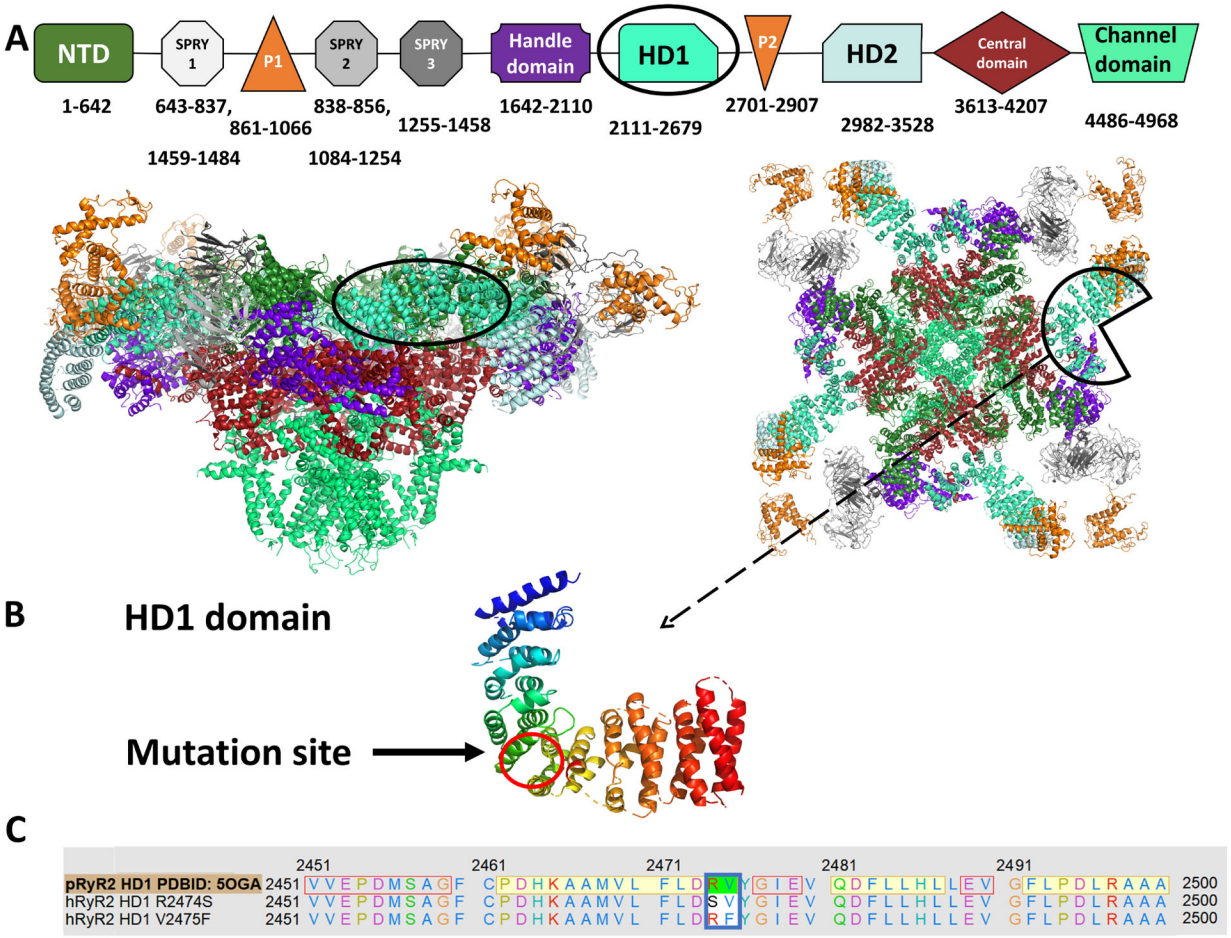

Figure 10. The location of the CPVT1 mutations R2474S and V2475F within the RyR2 structure

(A) Domain organisation of RyR2 and, below, side view (left) and cytosolic view (right) of the structure. **(B)** Zoom-in view of the HD1 domain indicating the location of R2474 and V2475. **(C)** Sequence alignment including the pig WT sequence corresponding to the structure (human sequence is identical in this region) and the R2474S and V2475F mutated sequences. The mutation sites are highlighted within the blue box and the secondary structure associated with the WT sequence is highlighted in yellow.

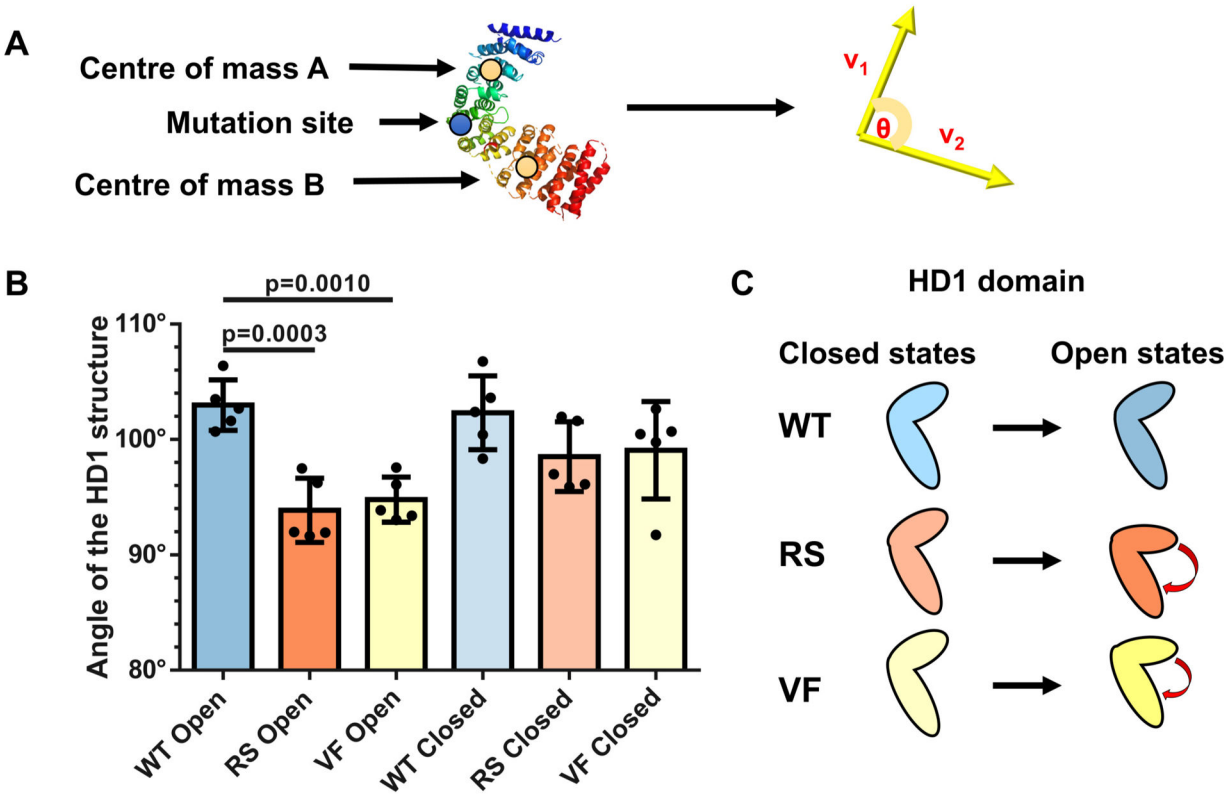

Figure 11. Modelling the effects of mutating R2474S and V2475F on the HD1 domain

(A) The HD1 domain is shown to demonstrate the approximate location of the R2474S and V2475F mutations (blue circle) and how the hinge angle was defined. The angle was calculated between the two vectors originating from the mutation site by dividing the HD1 domain into two parts, lobe A (residues 2111–2473) and lobe B (residues 2476–2679), connected by the mutation sites. The centre of mass (yellow circles) was calculated for each lobe as well as for the mutation site. **(B)** Bar chart illustrating the effects of the V2475F (VF) and R2474S (RS) mutations on the hinge angle. One-way ANOVA, p = 0.0002. Post hoc multiple comparisons with Tukey's correction comparing: WT and R2474S in open state p = 0.0003; WT and V2475F in open state p = 0.0010. Mean ± SD, n = 5. **(C)** Cartoon illustrating the bending of the RyR2 HD1 domain and reduced hinge angles of the mutants.

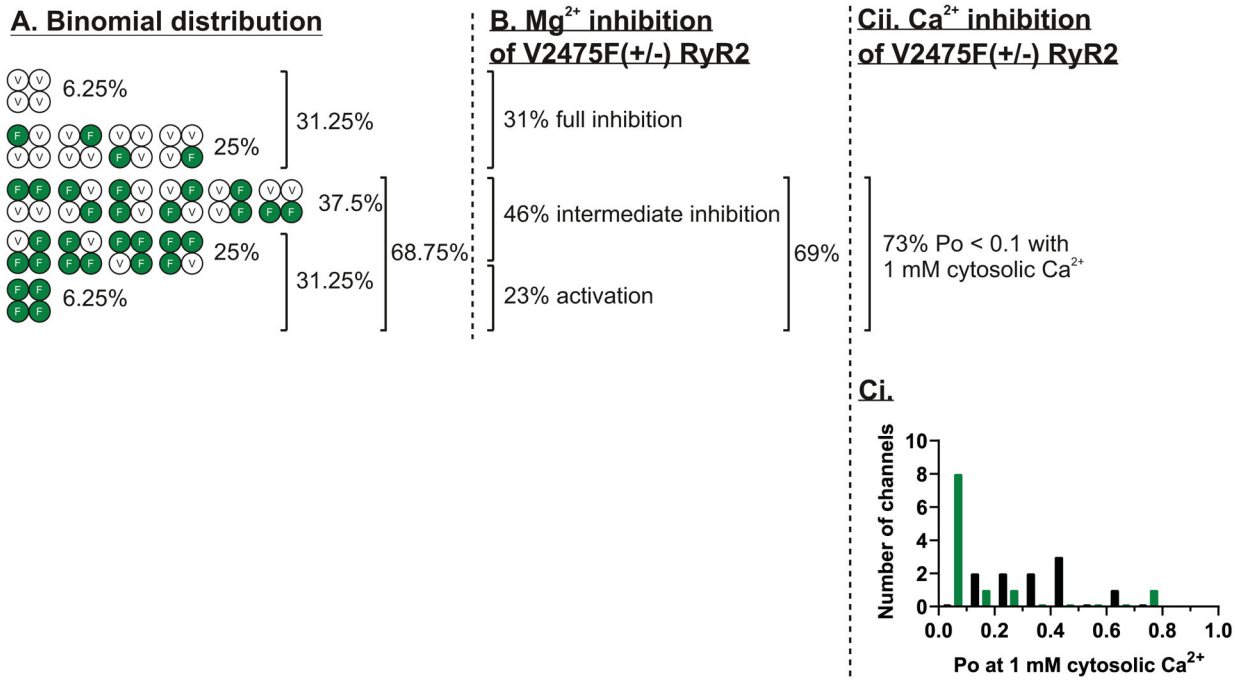

Figure 12. Likelihood of formation of RyR2 tetramers with different compositions of V2475F mutated monomers.

(A) White and green (F) circles represent WT and V2475F(+/−) mutated monomers, respectively. Assuming random assembly and identical surface expression, the probabilities of tetramers with the indicated numbers of mutant or WT subunits per tetrameric RyR2 channel is indicated as a percentage. **(B)** Data from Fig. 9, indicating the percentage of V2475F(+/–) channels exhibiting full inhibition (31%), intermediate inhibition (46%) or activation (23%) in response to cytosolic Mg^{2+}. **(C)** Data from Fig. 3, displaying (i) a frequency histogram for Po at 1 mM cytosolic Ca^{2+} and (ii) indicating the percentage of V2475F(+/–) channels exhibiting high sensitivity to inhibition by 1 mM cytosolic Ca^{2+}. (Po< 0.1 in the presence of 1 mM cytosolic Ca^{2+}).

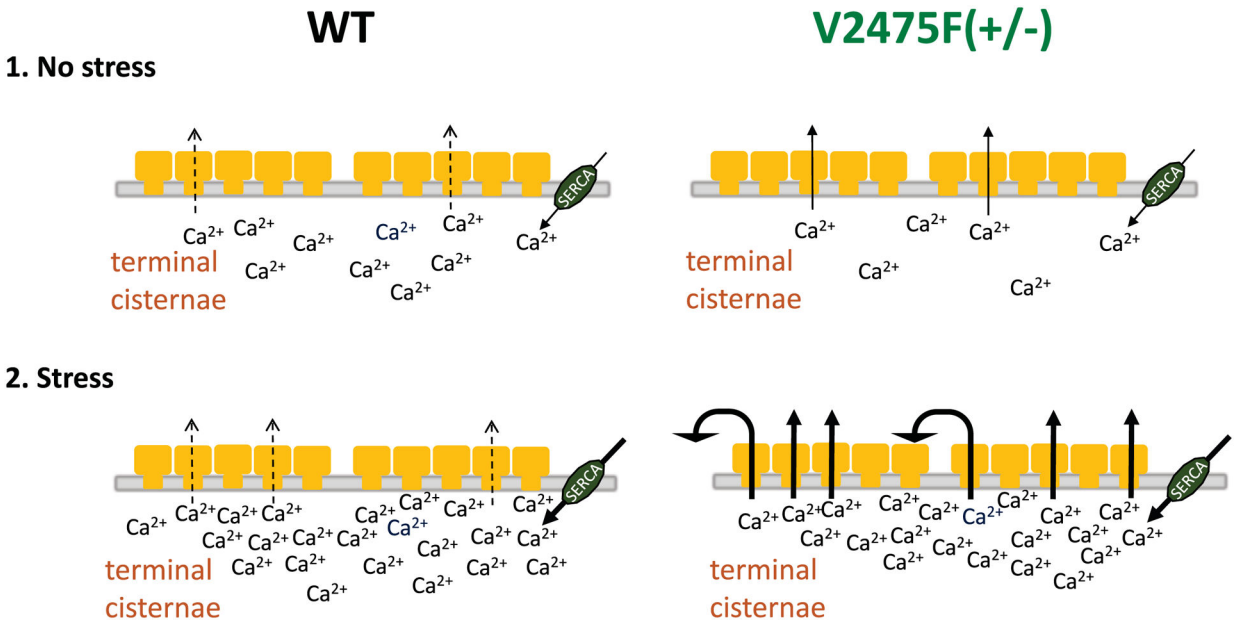

Figure 13. Model of the changes in diastolic SR Ca^{2+} release in V2475F(+/–) cardiac muscle cells

1. No stress Similar low numbers (14–20%) of WT or V2475F(+/−) RyR2 are activated during diastole at 100 nM cytosolic Ca^{2+} (Fig. 3B). V2475F(+/−) RyR2 channels open for longer durations (Fig. 3D) but it is expected that the increase in SR Ca^{2+} release will be transient (Kashimura *et al.*, 2010) as SR Ca^{2+} content will be lowered until equilibrium is achieved and net SR Ca^{2+} release reverts back to WT levels. Thus, DADs are not triggered.

2. Stress Adrenergic stimulation activates SERCA, causing increased SR Ca^{2+} content (Kashimura *et al.*, 2010) in both WT and V2475F(+/−) cells. SR Ca^{2+} binds to sites on the luminal side of RyR2 and potentiates the effects of ligands activating RyR2 from the cytosolic side (Sitsapesan & Williams, 1994a). At 100 nM Ca^{2+}, WT channels open with very low Po, and the potentiating effects of luminal Ca^{2+} are not significant until cytosolic Ca^{2+} is increased when Ca^{2+} enters through L-type Ca^{2+} channels during the action potential. In contrast, at 100 nM Ca^{2+}, V2475F(+/−) channels are already gating into long open events (Fig. 3D). In addition to this defect, V2475F(+/−) RyR2 are also exquisitely sensitive to slight increases in cytosolic Ca^{2+} (EC_{50} = 120 nM) (Fig. 3A) and a large proportion of V2475F(+/−) channels are insensitive to the inhibiting effects of the millimolar cytosolic Mg^{2+} present in cardiac cells (Fig. 9). It is therefore likely that the increased SR [Ca^{2+}] will potentiate the heightened stimulatory effects of cytosolic Ca^{2+} and Mg^{2+} to increase SR Ca^{2+} release causing Ca^{2+} waves and DADs. In spite of the increased number of spontaneous Ca^{2+}-release events in the V2475F(+/−) cardiac cells, there is no evidence that the SR Ca^{2+} content of the V2475F(+/−) cells is significantly lower than that of WT cells as evidenced by caffeine-induced SR Ca^{2+} release experiments by Loaiza et al. (2013) (Fig. 6C).

Table 1:

Burst analysis parameters at 100 nM cytosolic Ca^{2+}.

Unless otherwise stated, the parameters listed are calculated from all bursts. The p value was calculated by a Mann-Whitney test. n = 6 for WT, n = 10 for V2475F(+/−).

	WT	V2475F(+/−)	
PARAMETER	**MEAN ± SD**	**MEAN ± SD**	**p value**
Interburst interval (ms)	**1739.5** ± 1371.5	**1377.8** ± 1991.1	0.1806
Burst duration (ms)	**72.7** ± 82.7	**447.7** ± 497.3	**0.0420 ***
Burst duration with >1 event (ms)	**123.3** ± 118.5	**757.5** ± 950.6	**0.0312 ***
Burst duration of 1 event (ms)	**4.1** ± 3.0	**4.9** ± 6.8	0.5622
Intraburst open duration (ms)	**8.5** ± 3.3	**14.3** ± 18.6	0.7128
Intraburst closed duration (ms)	**9.6** ± 5.4	**18.0** ± 16.3	0.3132
Events in burst (n)	**9.4** ± 13.3	**19.8** ± 17.0	0.1179
Proportion of bursts with 1 event (%)	**55.0** ± 18.4	**39.4** ± 14.5	0.1806